University Carlos III Madrid

Bachelor Thesis

Ion Beam Shepherd: Analysis of the Plasma Bridge Interaction

Author: Rosario López Estergaard Jacobsen

Tutor: Filippo Cichocki

September 2015

Abstract

In the context of an exponential increase in the space debris population, which might yield to a substantial reduction of space activities in highly exploited orbits in a near future, new techniques for mitigating its growth are of key importance and are receiving an increasing attention in the international community. Among many proposals for active debris removal stands the Ion Beam Shepherd (IBS), a method which consists in a spacecraft rendez-vousing with the space debris object and relocating it to a different orbit with the use of electric propulsion. Such a shepherd spacecraft consequently requires two main thrusters, one directed at the target object, which transmits a force to it through the action of the ions of the plasma plume, and the other one, used to compensate the thrust generated by the first, thus maintaining the satellite and the debris at a constant distance throughout the de-orbiting or re-orbiting mission.

In this bachelor's thesis, the plasma interaction between the IBS and a target debris is studied through simulations. The software used for modelling the system and simulating its physics is SPIS (Spacecraft Plasma Interaction Software), an open source software developed by Onera and Artenum under the contract of the European Space Agency. Unfortunately, some unexpected technical issues with the software made it impossible to study, in detail, the primary goal of the differential charging between the IBS and the debris when a plasma bridge is established between the two objects. However, the corresponding limitations in the use of the SPIS software (not known a priori) were identified and its knowledge will certainly help any future project whose goal is to study the spacecraft-debris interaction in the context of the IBS.

Finally, some satisfactory results were obtained for the study of ions backflow towards the IBS satellite, which is relevant for the positioning of sensors and optical cameras on the surface of the spacecraft and also for the performance of its solar arrays.

Contents

List of Figures

List of Tables

Chapter 1

Introduction

Artificial satellites are nowadays very common, especially in the fields of communications, navigation, or meteorology. From 1957 onwards, approximately 6600 satellites have been launched, out of which around 3600 remain in orbit. Nevertheless, only around 1000 satellites are currently in use [10]. The remaining satellites are inactive and considered space debris.

Space debris, or space junk, is a definition that can be applied to any object orbiting our planet that is not carrying out a certain mission. This not only includes retired satellites, but also used up upper stages of rocket boosters that may remain in orbit, adding to the debris problem. Furthermore, it has occurred that remnants of fuel inside these boosters cause them to explode, creating a cloud of smaller sized debris. Fragmentation could ocassionally occur to satellites, either due to disintegration or collisions. This constitutes over 60 % of the catalogued objects in low Earth orbit (LEO). Other less frequent sources of space junk are lost equipment from missions or the use of anti-satellite weapons, as occurred in 2007 when China successfully tested an anti-satellite missile with one of its own defunct weather satellites, FengYun 1C, generating over 35,000 fragments of debris [11].

Currently, there are more than 21 000 objects longer than 10 cm catalogued by the US Space Surveillance Network as space debris. This large amount of space junk orbiting the Earth poses important threats to manned and unmanned spacecraft and even to the surface of our planet. As the debris orbits at velocities that are around 7 km/s [12], the impact of even small particles can damage a spacecraft provoking the end of its mission and, in the case of manned spacecraft, loss of life. In fact, NASA chief scientist for orbital debris, Nicholas Johnson, stated that "the greatest risk to space missions comes from non-trackable debris" [13]. However, collisions with large defunct objects have also occurred and these incidents are not only catastrophic to the implicated spacecraft, but also generate large amounts of fragments, which exacerbates the space debris problem.

Current satellite launch rates are around 70 new spacecraft per year and historic rates of spacecraft break-ups are close to five per year [1]. If these

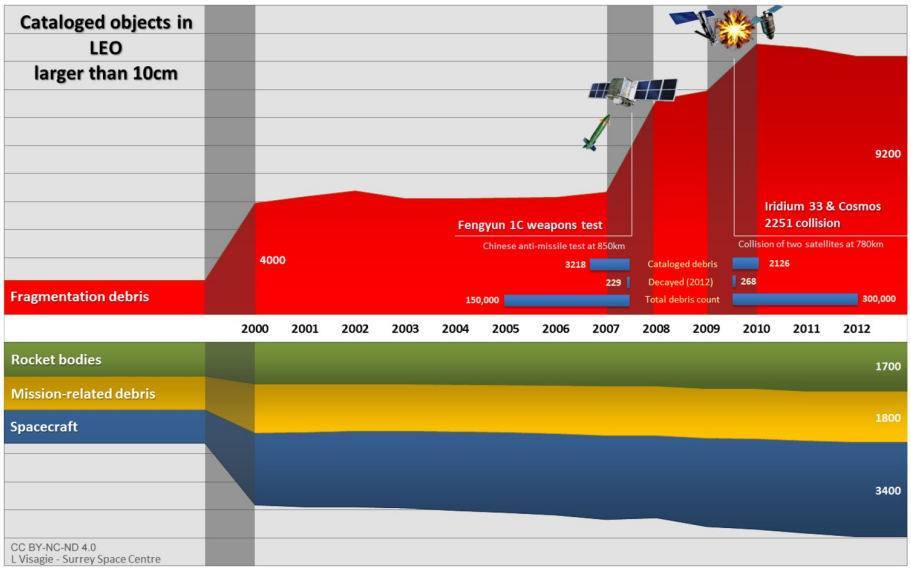

Figure 1.1: Space debris in LEO larger than 10 cm. Source: Surrey Space Centre

figures are maintained, the amount of space junk shall continue to increase. The commonly known "Kessler Syndrome" states that the increment of artificial satellites orbiting our planet will raise the probability of collisions among them. These collisions would result in a large number of fragments entering in orbit, each of which would further increase the probability of collisions. This could eventually lead to a worst-case scenario of a belt of debris surrounding our planet rendering space missions in LEO unviable [12].

NASA has made predictions related to collisional events among objects in LEO larger than 1 cm [14]. The study foretells an overall increase in the collision rate, reaching a value of four events per year by the end of 2035, being non-catastrophic collisions the dominant mode of collisions. This study assumes that standard mitigations techniques, successful upper stage safing and mission-related debris suppression, are maintained throughout the study period.

However, in order to avoid the runaway effect that could result from collisions with orbiting debris, the measures that are currently taken are not enough. Fig.1.2 shows the evolution with time of the number of space debris larger than 10 cm predicted by the LEGEND model [1]. From the plot, it becomes clear that simple post mission disposal (PMD) guidelines, which require payloads and upper stages to be removed from orbit in a maximum of 25 years after the end of their operational life, are not sufficient to impede the growth of catalogued objects in LEO. If combined with active debris removal (ADR) however, predictions are more optimistic, reaching an almost constant trend when 5 objects are removed from orbit per year .

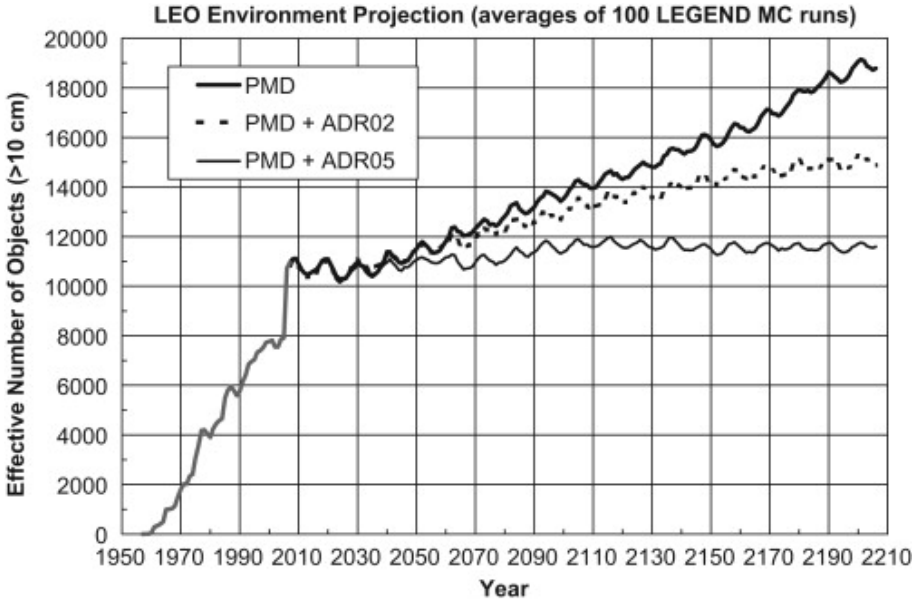

Figure 1.2: LEGEND model predictions of the number of catalogued objects for 3 scenarios: PMD only, PMD plus ADR of 2 objects per year, and PMD plus ADR of 5 objects per year. Source: [1]

Mitigation of space debris can be divided in near term measures and longer term measures.

Near term measures include actions such as limiting the debris released during normal operations, if possible reducing it to zero, and minimizing the potential for break-ups. Passivation techniques have been, up till now, the most effective way to avoid post-mission explosions. This consists of releasing all residual energy reservoirs of a spacecraft or orbital stage. 'Design for Demise' is also a short term mitigation method that relies on an intentional design to assure that the spacecraft will fragment in the required way during re-entry.

In the long term, the most effective mean appears to be the removal of mass from the region of high density of space junk. This should be done by removing the object from orbit in a controlled manner, or, if not possible, displacing it to a graveyard orbit above 2000 km for LEO orbits and above 36000 km for GEO orbits, to avoid its interference with commercial or scientific orbits.

The removal of mass from highly populated orbits can be executed by the object itself (PMD) or by an external spacecraft (ADR).

The simplest of self-removal techniques consists of the rocket stage or satellite powering itself to an orbit that reduces the de-orbiting time or to a graveyard orbit. This has been successfully carried out with the French Spot-1 satellite in 2003 [15]. As this implies allocating part of the payload of the mission to fuel, which is expensive, other methods that avoid the use of propellants, like passive

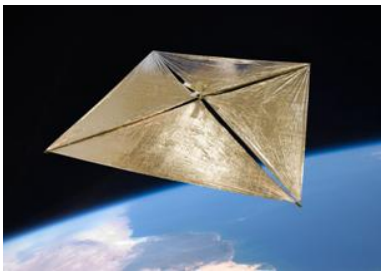

Figure 1.3: Artist's recreation of NanoSail-D deployed in orbit. Source: NASA

de-orbiting methods, have been studied. The most relevant is the use of sails that deploy from the spacecraft in order to benefit from the aerodynamics drag that is experienced in LEO, as illustrated in Fig.1.3. In 2010, NASA launched the NanoSail-D2 [16], which proved the correct functioning of the sail drag removal method. Another de-orbiting technique, currently under investigation, makes use of the Lorentz force fruit of the interaction of the Earth's magnetic field and the current that is generated by an electrodynamic tether [17].

Though these techniques can be easily carried out, not many of the currently orbiting objects include PMD. As a consequence of this and the fact that the current LEO environment is already over a critical space debris density, active debris removal is a necessity.

ADR proposals are numerous and varied. The most common procedure is to capture the debris with a remotely controlled vehicle and then drag it to an orbit from which it shall be de-orbited by the atmospheric drag more quickly. This is the base of the Orbital Debris Remover, ORDER, designed by the private company Busek, that proposes the ORDER spacecraft to deploy a smaller spacecraft named *Satellite on an Umbilical Line*, SOUL, to attach to the debris. ORDER would then fire its thrusters to relocate the object [18].

Nevertheless, this approach to external removal is complicated, as it requires control of the attitude not only of the docking spacecraft, but also of the debris. In contrast, there are proposals for low-risk manipulation of the object to be de-orbited such as the use of harpoons, nets (studied by ESA for the 2021 e.DeOrbit mission [19]) or even contactless manipulation.

This is the case of using an expanding foam to remove debris. This proposal from the University of Pisa, approved by ESA, consists of shooting the debris with a polymeric foam that will expand isotropically to form a sphere that covers part of the target [20]. This increase in surface shall accelerate the de-orbiting process due to an increment in drag.

Another contactless active debris removal method is the Ion Beam Shepherd (IBS) presented by the Polytechnic University of Madrid [4]. This method consists of a shepherd spacecraft that actively controls the target's orbit. Momentum is transmitted from the shepherd to the debris through a beam of quasi-neutral plasma that is impinging against the debris surface. Another electric thruster is required for the shepherd to maintain a constant distance from

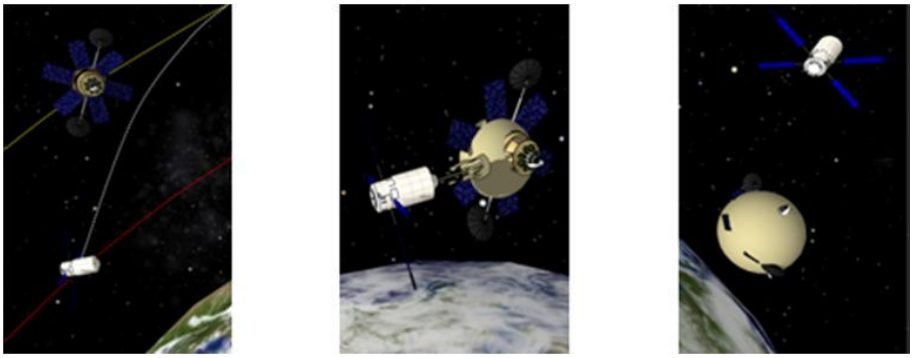

Figure 1.4: De-orbiting through foam expanding foam application. Source: University of Pisa

the target while "pushing" it out of orbit. A more thorough description of the IBS is presented in Chapter 2.

Chapter 2

The IBS Concept

2.1 Description of the Concept

The ion beam shepherd, as previously mentioned, is a proposed technique for active debris removal that avoids contact with the debris. The base of its functioning is the "shepherd", a spacecraft with the mission to control the orbit of a large target by directing a beam of ions towards it. This beam would be generated by an electric propulsion system.

The principle behind electric propulsion is the creation and the subsequent acceleration of ions, by an electric or electromagnetic field, so as to excert a reaction force on the spacecraft in the direction opposite to the ejection of the ion stream. This ion stream must then be neutralized by constantly emitting an equal current of electrons with a "neutralizer". The IBS proposes the usage of the beam of ions in the alternative manner mentioned previously.

In Fig.2.1 it is possible to observe that more than one electric propulsion systems are used, specifically three. They are the Impulse Transfer Thruster (ITT), the Impulse Compensation Thruster (ICT) and the Reaction Control System (RCS).

The ITT is the most fundamental part of the mission as it is the one that supplies the target debris with an impulse. It is used throughout the complete shepherding phase and turned off otherwise. Specific requirements of the ITT shall depend on the objective to remove (size, mass and orbit). However, common requirements such as low plume divergence, high specific impulse or a long lifetime incite the use of electric propulsion for this thruster.

The main objective of the ICT, as its name suggests, it to compensate the reaction force generated on the spacecraft by the ITT. This is necessary in order to maintain a constant distance between target and shepherd. The ICT is also the engine in charge of orbit transfer and phasing maneuvers. Once again, requirements related to high specific impulse and long lifetime suggest the use of electric propulsion.

Finally, the RCS is necessary to provide three degrees of position and at-

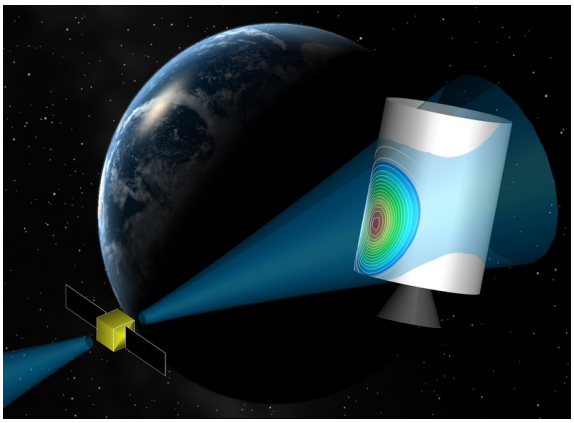

Figure 2.1: Illustration of the IBS in action. Source: LEOSWEEP project at the Polytechnic University of Madrid

titude control of the spacecraft. It should be used in case of collision avoidance manoeuvres or any other safety manoeuvres. As these actions must be performed in a swift manner, chemical propulsion seems better suited for this system. However, the ITT might be used to control the degree of freedom along the S/C - debris line, allowing the RCS to be used more for lateral control, which can be achieved with electric propulsion as well.

To further introduce the IBS, an insight on the dynamics of the shepherd-target system shall be provided. Fig.2.2 shows the distribution of forces of the system, where $\boldsymbol{F_{ITT}}$ is the Impulse Transfer Thruster thrust and $\boldsymbol{F_{ICT}}$ is the Impulse Compensation Thruster thrust. The force acting on the target is given by:

$$\boldsymbol{F_D} = \eta_B \boldsymbol{F_{ITT}} \tag{2.1}$$

where η_B is the beam momentum transfer efficiency. This efficiency is the ratio between the axial component, along the direction of the beam, of force that is transmitted to the target and the total ITT thrust:

$$\eta_B = \frac{F_Z}{F_{ITT}} \tag{2.2}$$

The efficiency shall be dependent on beam-target interaction geometry and the distance between shepherd and debris. To maximize the efficiency, the distance must be minimized, as this decreases the divergence the plume experiences before reaching the target. Nevertheless, a compromise must be found between high efficiency and interbody safety constraints [4]. Typically, the minimum distance is set by the shepherd's half span to guarantee that, even in the event of a total relative navigation failure, no collision would occur.

The effect of the ICT becomes relevant when calculating the total force acting on the shepherd, which is given by:

$$\boldsymbol{F_S} = \boldsymbol{F_{ICT}} - \boldsymbol{F_{ITT}} \tag{2.3}$$

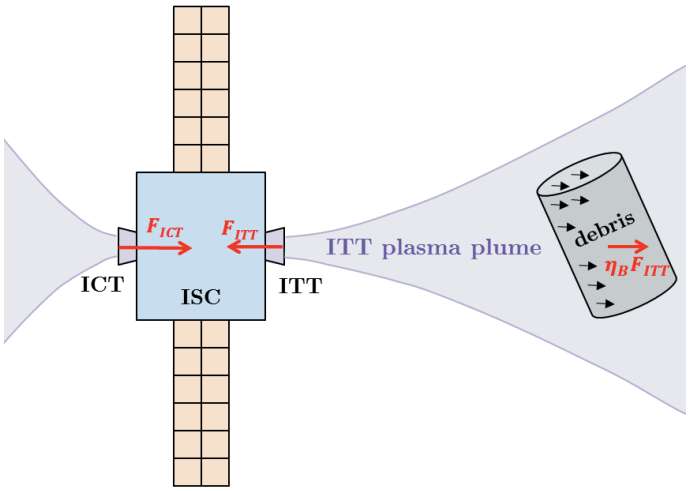

Figure 2.2: Schematic of the IBS functioning. Source: [2]

This force will define the motion of the spacecraft and shall be related to the force acting on the debris as both objects must be maintained within a certain distance of each other. This implies that, during deorbiting the acceleration of the debris and spacecraft must be the same:

$$\frac{F_D}{m_D} = \frac{F_S}{m_S} \tag{2.4}$$

From this expression, it is possible to obtain a relation between the required thrust of the two main engines by applying Eq.2.1 and Eq.2.3 and operating to obtain the following:

$$\frac{F_{ITT}}{F_{ICT}} = 1 + \eta_B \frac{m_S}{m_D} \tag{2.5}$$

2.2 Comparison with Other Mitigation Methods

The Ion Beam Shepherd is an active debris removal method that acts in order to mitigate the space debris situation. However, many other mitigation methods have been developed. This section provides a comparison between the IBS and other mitigation methods and a summary of the former in table 2.1.

First of all, the IBS is a system designed to remove objects that are already orbiting without control. Therefore, it falls into the category of active debris removal, which differs from other mitigation techniques in the sense that it requires the debris to be already existent. It is a remedial measure, in contrast to preventive measures such as passivation, "Design for Demise" or systems

that are embedded in the initial design of the future debris (sails, balloons or electrodynamic tethers).

A key aspect that characterizes the IBS is that it is a contactless method. This is a great advantage as it eliminates the need for docking with a non-cooperative object, as required by techniques involving robotic arms or tentacles. Additionally, avoiding physical contact with the debris reduces the risk of fragmentation due to collision or explosion in the target's batteries and propellant tanks, which is also a risk in soft mechanical interface methods such as those based on the use of nets or harpoons. However, the lack of contact with the target difficults controlling it during re-entry into Earth's atmosphere. As the electric propulsion of the IBS excerts a very small force on the debris, re-entry trajectory cannot be precisely controlled. This presents a problem for objects heavier than 500-1000 kg [21] that shall be discussed in more detail in the next section of this chapter. However it is interesting to note that the IBS is capable of completely de-orbiting any target, though this implies that the satellite is lost in the process and can not de-orbit more than one object.

ADR methods may be classified in terms of their strategy for debris removal as *one-to-one*, if the deorbiting spacecraft must be designed for a specific target; *one-to-many*, if the spacecraft is able to de-orbit several objects in each mission; or *one-to-any*, if the spacecraft may de-orbit any one debris in each mission. By this classification, the IBS can be described as a one-to-many ADR. This is a common approach shared with electromagnetic methods, the use of nets or the expanding foam-based method. As debris tends to concentrate at certain altitudes (Fig.2.3) and orientations, to accelerate the process of cleaning high-density orbits, a multiple-target approach appears to be feasible and better suited. However, de-orbiting missions with a single target are also being taken into account, as these missions provide benefits in terms of simplicity and are propitious to demonstrate the correct functioning of the designed technologies.

Another distinction that can be made between ADR methods is depending on their target size. The IBS aims for large orbital debris, as these objects present extremely important threats if a collision were to involve them. Thus, removing them from orbit shall mitigate, in the long run, the formation of further space debris due to fragmentation or collision. This is the priority of most of the previously mentioned ADR, mechanical arms, tentacles, harpoons or the IBS, that are designed to de-orbit one object at a time. Nonetheless, from a current perspective, not only large debris present a threat. Small objects between 1 to 5 cm have an important probability of impacting with a spacecraft and causing loss of functions or missions [21]. A proposal to eliminate this sector of debris consists in the use of lasers (ground, air or space-based) to slow debris down and in this way alter its trajectory.

Finally, the IBS may be compared to other mitigation methods in terms of technological readiness level (TRL).

In contrast to actions such as passivation or "design for demise", that were already included in guidelines for space debris mitigation set by the United Nations in 2010 [22] and are, therefore, ready for application, all active debris removal methods present a challenge. Though some of the required technologies

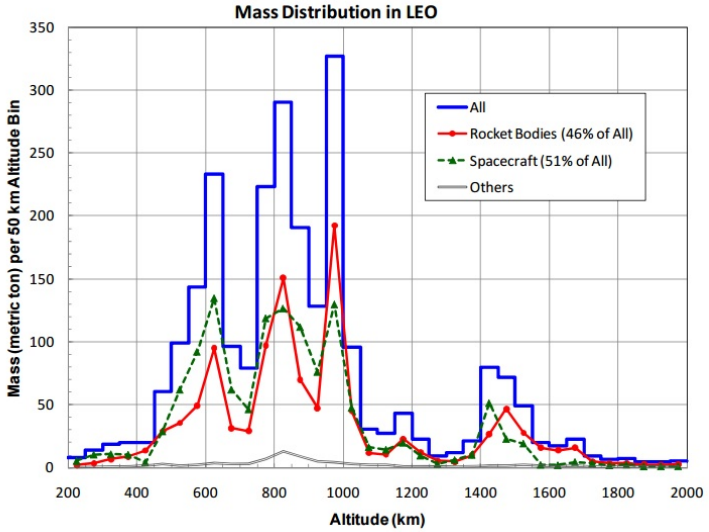

Figure 2.3: Density of orbital debris with respect to altitude. Source: [3]

exist at present and have proved successful, they still require adaptation to debris removal purposes and in some cases, a reduction in cost to render ADR missions feasible.

A common factor among most ADR techniques, including the IBS, is the performance of a close-range rendez-vous with a non-cooperative object. This requires advances in sensor technology, propulsion systems and guidance, navigation and control (GNC) capabilities that are currently being studied [19]. But, for example, as the IBS is a contact-less method, it is not dependent on the readiness level of de-tumbling mechanisms that are required in ADR systems that are in contact with the target.

In general, comparison with other proposals to clean highly populated orbits does not set the IBS significantly behind in TRL. Nevertheless, improvements in many fields are required before the technique is ready for use. The LEOSWEEP project([4],[23]) aims at increasing the IBS' TRL significantly, targetting a series of aspects that complicate its development. Some of these issues are presented in the following section.

2.3 IBS Major Issues

Throughout the investigation on the IBS carried out up till now, several aspects have been found to possibly hinder its efficient functioning. The main issues that have arisen are discussed below.

Method	Pros	Cons
Nets	- No complex docking - Can handle any shape, attitude or spin rate	- Heat resistant materials required as thruster plume is directed towards the net - Potential fragmentation
Harpoons	- No complex docking - Can handle any shape, attitude or spin rate	- Difficulty of harpoon to penetrate object - Anchor strength once penetration is achieved - Potential creation of more debris if energy storage is pierced or due to fragmentation
Clamping	- Ability to control re-entry into Earth's atmosphere	- Risk of exploding debris' energy stores - Risk of collision or fragmentation - Requires great precision during rendez-vous and capture
Foam	- No complex docking - No control required for re-entry	- Specific storage requirements - Risk of leakage inside spacecraft
IBS	- No complex docking - High de-orbiting efficiency due to use of electric propulsion	- No controlled re-entry

Table 2.1: Comparison between ADR methods.

Effects of Geomagnetic Field

The Earth is surrounded by a magnetic field generated by the electric currents that exist in its core, which is a conductive material. The potential influence of this field on the plasma beam of the IBS is a topic of concern.

There is a tendency for electrons to follow magnetic lines unless they collide or some drift displaces them. Though the geomagnetic field at LEO is weak (approximately 0.5 Gauss), the far field plume presents few collisions. Consequently, there exists the possibility of the plasma plume deforming due to the magnetic field, which could be an impedement to applying plasma beams to active debris removal.

Studies [24] expect a deformation of the cross-section of the plume a few metres from the thruster. This deformation would consist of an expansion in the direction parallel to the magnetic field and a reduction in the perpendicular direction. Nevertheless, these studies do not take into account the effect of the magnetic field that is induced by the plasma as a reaction to the external field. The internal magnetic field dominates in the core of the plume and as it opposes the geomagnetic field it should allow the core of the plasma beam to expand unperturbed [25]. However, at the time being, there is no experimental evidence that rules out the plasma plume deviation caused by the magnetic field. It is, therefore, an objective of the LEOSWEEP project to provide a reasonable answer for this.

Ion Backscattering and Backflow

A critical aspect of the IBS concept is the backsputtering of particles. This phenomenon occurs when atoms or clusters of atoms are removed from the debris material by the energy of the impinging plasma beam. A small percentage of the sputtered atoms are ionised and consequently they are subjected to the electric field that is generated between shepherd and target.

These ions pose an important threat to the mission because, if they were to settle on sensitive surfaces of the shepherd satellite, they may interfere with their correct functioning. The surfaces that are most prone to degradation due to backsputtering are the cover glass of solar cells and thermal control materials, as they are most abundant on the spacecraft's surface [26]. Furthermore, the contamination of an optical sensor also generates a serious problem.

A form of reducing backsputtering is to reduce the divergence of the plasma plume. This measure allows for a larger operational distance between shepherd and target without losing momentum transfer efficiency, which in turn implies that a smaller backflow is received. It can be seen from Fig.2.4 that a reduction in beam divergence angle of the order of 10 ^{o} will produce a decrease in backsputtering flux of approximately one order of magnitude.

Another source of backflow are charge exchange collisions (CEX). Although electric propulsion systems such as ion engines have a high ionization efficiency, not all of the propellant is ionized. As the remaining neutrals are not accelerated by electrostatic forces, but instead leave the thruster at a thermal velocity

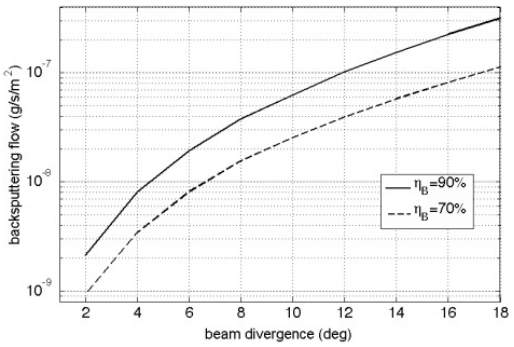

Figure 2.4: Backsputtering flow reaching the IBS spacecraft from an aluminium spherical target with respect to deam divergence angle for momentum transfer efficiencies of 90% and 70%. Source: [4]

significantly lower than the ions' exit velocity, a higher density of neutrals compared to fast ions is present in the near region of the plume, promoting CEX collisions in this region. The result of a CEX collision is that a slow neutral sheds an electron to a fast ion converting it into a fast neutral, which is of no importance as it has lost no momentum. However, the slow ion that is left behind is more susceptible to local electrostatic forces that accelerate it radially away from the plume and towards the spacecraft, contributing to contamination and erosion of delicate surfaces and differential charging of the satellite [27].

It is important to mention also the other side of the story, which involves the erosion of the target due to sputtering. Though in general it is expected that the ion beam have a minimal erosion effect on the target, it is necessary to ensure that the structural integrity of the debris is not compromised and no further generation of debris will occur.

Onboard Power Limitations

The IBS requires at least two electric propulsion systems on board, the impulse transfer thruster and the impulse compensation thruster. As a small time of deorbiting of each objective would maximize the amount of debris the IBS could remove in a single mission, a high specific impulse is desired for these thrusters. However, large specific impulse implies a high power consumption. Considering that the IBS employs two thrusters, the power generated by the shepherd's solar panels may not be enough to provide the required thrust levels at the desired specific impulse. A compromise must be reached for the mission to be possible.

The IBS project has been developed considering ion engines as a possibility for the propulsion system, as this type of engine has a reduced beam divergence in comparison to Hall-effect thrusters. A recent ion thruster design with 4 grids named DS4G presents beam divergence lower than 6 ^{o} [28], which is consider-

ably lower than conventional ion engines. Nevertheless, the operating voltage to achieve such a small divergence angle is quite high (up to 5 kV) and would yield an excessive power demand for a simple IBS demonstration mission. Thus, simple two-gridded ion engines have been chosen as the most promising candidates for the IBS's propulsive system. In any case, a specific optimization of both the ITT and ICT is, in general, necessary in order to maximize the efficiency of this ADR method [2].

Uncontrolled Re-entry

Approximately 10-20 % of the mass of the large objects that are top priority in the removal of space debris will possibly survive re-entry into the atmosphere [21]. The fragments that remain may pose a risk to people or property. Furthermore, as the momentum transferred by the IBS to the debris is low, it is difficult for the angle of incidence of re-entry to be larger than approximately 1 °. This, combined with the fact that the major break-up occurs at an altitude of 80 km, implies that the footprint of the re-entry is long and predicting the location of impact is not possible [29].

This drawback of the IBS makes the system more suited for re-orbiting debris that ir in Geostationary orbits (GEO) as proposed by Kitamura in [26]. However, it is in no way a show-stopper for the IBS concept applied to debris removal in LEO, where the need for ADR is more pronounced. A possible solution is to de-orbit the target to a determined altitude where another ADR method may step in and finish the process. A solid propellant de-orbitation kit consisting of a solid rocket engine with an end-burning grain configuration, could be clamped to the target and then fired, providing the ΔV necessary to enter the atmosphere over a remote area half an orbit later [19].

2.4 Open Investigation Areas

The IBS concept is still under development, which implies that there are several aspects that must be investigated before its testing on a real demonstration mission. Investigation is centred mainly on the expansion of the plasma plume and on the interaction between the shepherd spacecraft and the target debris.

The plasma beam generated by the electric propulsion systems may interact with the rest of the spacecraft producing detrimental effects such as contamination of sensitive surfaces, charging of the spacecraft or even a limitation in electromagnetic communications. The importance of a thorough study of the expansion of the plasma plume in vacuum is, therefore, crucial. As experiments for this require a large financial expense and they are also limited in the reliability of their results due to the finite size of vacuum chambers or the residual gas pressure, numerical simulations are the most effective way to analyze the problem at the moment.

The plasma plume is characterized by two distinct regions: a near region plume close to the thruster exit, where the local electric fields and the electric

fields due to charge-exchange collisions dominate; and a far region plume which is quasi-neutralized and dominated by the residual plasma pressure. The former is generally simulated with particle based tools, while the latter requires a two-fluids model. Several methods for this, such as the asymptotic expansion method and the self-similarity method, have been applied to the IBS and compared, presenting both advantages and disadvantages. [30]. However, these semi-analytic models can be limited in characterizing physical processes. To compensate for this drawback, an advanced 3D fluid/particle-in-cell (PIC) code, EP2-PLUS, is being developed at the Carlos III University of Madrid [25].

The advanced code proposed will study 3D phenomena such as the interaction with the Geomagnetic field and also the relative charging between the spacecraft and debris. It shall not limit its area of interest to the central plume, but also describe the lateral region of the plume, which becomes of importance when studying the ion backflow and backsputtering problems. In this manner, it targets the two main foci of investigation required for the IBS project.

Finally, a technological improvement that is fundamental for an efficient realization of debris removal with the IBS is the reduction of plume divergence. This will allow for an increased momentum transfer efficiency while permitting a separation between target and shepherd large enough to avoid collision risks and to weaken the effect of backsputtering.

2.5 Objective of the Thesis

The objective of this thesis is to study the plasma interaction between the IBS and the target debris in terms of the mutual charging, known as the plasma bridge, and of the ion backflow towards the shepherd. Evaluating these two phenomena is a very important step towards testing the IBS technique in a real demonstration mission. The study shall be carried out through simulations using the open-source software SPIS (Spacecraft Plasma Interaction Software) developed by the French companies Onera and Artenum under ESA's contract [9], [31].

Chapter 3

Plasma Basics and Simulation

A definition of plasma and an introduction to its basic equations are fundamental in this work as its object of study, the plasma bridge between the IBS and its target debris, is clearly made out of plasma.

Thus, it seems reasonable to begin by defining plasma as an ionized gas. This state, referred to as the "fourth state of matter", is reached when a gas is heated to the point where collisions between highly energetic atoms or between atoms and highly energetic electrons remove an electron from the atoms' outer shell, producing an ion-electron pair. The motion of electrons and ions can produce both electric currents and electric fields as a consequence of the separation of charges.

As a collective, plasma tends to be almost electrically neutral. This is the result of the restorative electric field that appears when a net charge density starts to build up inside the plasma. A plasma composed of singly-ionized ions being electrically neutral implies that, because the charge of ions and electrons is equal in magnitude but opposite in sign, it has approximately the same density of ions and electrons, $n_i \approx n_e$. This condition is fulfilled in all the volume of plasma with certain exceptions, which are presented in the following section.

3.1 The Plasma Sheath

Electrons have a tendency to gather close to positive charges in a plasma, while ions behave in the opposite manner, gathering close to negative charges. Furthermore, electrons are much more mobile than ions (due to their much smaller mass) and, therefore, can escape the plasma much faster. These two effects combine to produce a plasma bulk, which is generally quasi-neutral, and a net charge accumulation only close to the plasma boundaries, where electric fields build up to maintain the plasma equilibrium. This net charge region has a linear size, which represents a fundamental property of a plasma: the Debye length.

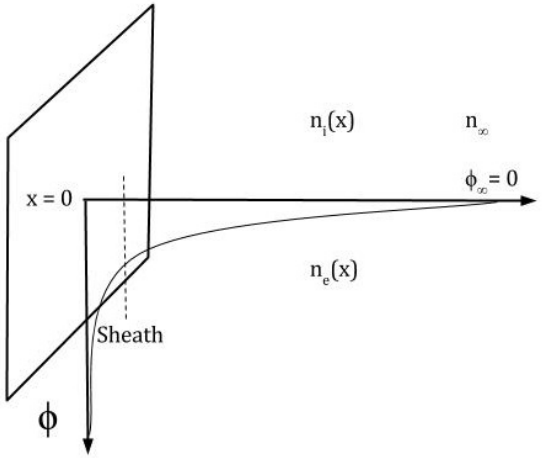

Figure 3.1: Schematic of the potential distribution for calculation of the Debye length.

Such length represents the distance over which, charge accumulation yields to an almost complete electric shielding of an external electric disturbance (e.g. an immersed biassed conductor, an external wall, etc). For the plasma to be quasi-neutral, the size of the Debye length must be much smaller than the size of the plasma.

For a simplified or idealized system, the calculation of the Debye length proceeds as follows. The boundary conditions state that at infinity (in the bulk plasma far from the electric disturbance source) the density of electrons and ions are equal $n_e = Zn_i \equiv n_\infty$ and that the potential is equal to zero $\phi_\infty = 0$, as can be seen in Fig.3.1. Here, Z represents the ionazation state of the ions, being 1 for singly charged ions. The density as a function of position can be defined from the Boltzmann factor:

$$n_e(x) = n_\infty \exp\left(\frac{e\phi(x)}{T_e}\right) \tag{3.1}$$

$$Zn_i(x) = n_\infty \exp\left(\frac{-eZ_i\phi(x)}{T_i}\right) \tag{3.2}$$

where e is the charge of an electron and T_e and T_i are the temperatures of electrons and ions respectively. These temperatures are assumed to be different, though spatially homogeneous. This implies that the ions are in thermal equilibrium amongst themselves, as are the electrons, which is frequent in plasma due to the large difference in mass between the particles.

The densities may now be introduced into Poisson's equation, Eq.3.3:

$$\nabla^2\phi = -\frac{\rho}{\epsilon_0} = -\frac{e}{\epsilon_0}\left(Zn_i - n_e\right) \tag{3.3}$$

where ϵ_0 is the permittivity of free space. Applying the Poisson equation to a one-dimensional planar geometry and assuming that the ions are singly charged ($Zn_i = n_i$), it is possible to obtain the following expression:

$$\frac{d^2\phi}{dx^2} = \frac{e}{\epsilon_0}(n_e - n_i) = \frac{en_\infty}{\epsilon_0}\left[\exp\left(\frac{e\phi}{T_e}\right) - \exp\left(\frac{-e\phi}{T_i}\right)\right] \tag{3.4}$$

By assuming that the perturbation in potential is small, $e\phi \ll T$, a Taylor expansion of the exponential terms may be performed, yielding Eq.3.5.

$$\frac{d^2\phi}{dx^2} \approx \frac{e^2 n_\infty \left(1 + T_e/T_i\right)}{\epsilon_0 T_e}\phi \tag{3.5}$$

The solution to this differential equation is a potential of the form:

$$\phi \propto \exp\left(\frac{-x}{\lambda_D}\right) \tag{3.6}$$

where λ_D is the Debye length:

$$\lambda_D = \sqrt{\frac{\epsilon_0 T_e}{n_\infty e^2\left(1 + T_e/T_i\right)}} \tag{3.7}$$

Considering a process timescale that is negligible with respect to the ions' mobility, the ion term in Eq.3.4 can be discarded and the final expression for the Debye length is reduced to:

$$\lambda_D = \sqrt{\frac{\epsilon_0 T_e}{n_\infty e^2}} \tag{3.8}$$

It is important to note that the temperatures introduced are in electron volts. If they were to be used in Kelvin, the conversion is performed using Boltzmann's constant, $k = 8.6173324 \times 10^{-5}$ eV/K.

As mentioned at the beginning of this section, sheaths do not form only around objects immersed in a plasma (as in this example), but also at the boundaries of a plasma. Electrons, due to their high mobility, are quickly lost through the boundary at the time of the plasma formation, consequently producing a potential drop, which hinders additional electron outflow, while favoring the ion outflow. For a dielectric container (no net current to the walls), stationary conditions are characterized by a potential drop such that equal ion and electron fluxes are lost through the boundaries. Equating the ion and electron fluxes, it is possible to extract the stationary value of the potential at the wall according to:

$$\phi_w = -\frac{k_B T_e}{e}\left(\ln\sqrt{\frac{2\pi m_e}{m_i}} + 0.5\right) \tag{3.9}$$

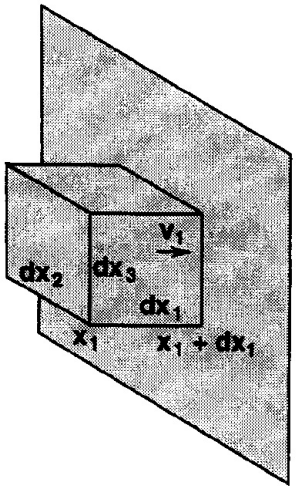

Figure 3.2: Differential element of volume considered for conservation of mass. Source: [5]

3.2 Two-fluid Plasma Model

Plasma may be analized as a collection of individual particles. However, this approach may result cumbersome and time-consuming. For this reason, it is interesting to develop a more statistical approach, considering an ensamble of particles with a fluid-like behaviour.

Any fluid model has a series of properties that are worth remarking. First of all, fluids are essentially three dimensional. Second, the variables that are dealt with are averaged over space. For the case of a plasma, these averaged properties include the density of particles ($n_i(\boldsymbol{r},t)$, $n_e(\boldsymbol{r},t)$), the average velocity of particles ($\boldsymbol{u_i}(\boldsymbol{r},t)$, $\boldsymbol{u_e}(\boldsymbol{r},t)$), pressures ($p_i(\boldsymbol{r},t)$, $p_e(\boldsymbol{r},t)$) and temperatures ($T_i(\boldsymbol{r},t)$, $T_e(\boldsymbol{r},t)$). Finally, it is important to state that even though the fluid model is less accurate and complete than the particle approach, the use of a fluid model is frequent and it is a choice based on simplicity.

Having introduced the fundaments of any fluid model, the most basic fluid model applied to plasmas will be derived below.

Conservation of Mass

To derive an equation for the conservation of mass of the particles contained in a plasma, a differential element of volume as depicted in Fig.3.2 is considered. The three coordinate directions, x_1, x_2 and x_3, are parallel to the sides of the volume element.

The number of particles flowing out of the volume element through the

surface shown in Fig. 3.2 per unit of time is given by:

$$\frac{\partial n}{\partial t}|_{x_1+dx_1} = n\boldsymbol{v_1}dx_2dx_3 \tag{3.10}$$

where $\boldsymbol{v_1}$ is the average velocity in the direction perpendicular to the plane that is being considered, the x_1 direction. Similarly, the number of particles flowing into the volume is given by the same expression as in Eq.3.10, but evaluated at x_1.

If the inward and outward flux of particles are summed the flow of particles across all of the six sides of the infinitesimal volume is obtained:

$$\frac{\partial n}{\partial t}d^3x = -\left(n\boldsymbol{v_1}dx_2dx_3\right)_{x_1+dx_1} + \left(n\boldsymbol{v_1}dx_2dx_3\right)_{x_1} + \dots \tag{3.11}$$

with $d^3x = dx_1dx_2dx_3$. Dividing this expression by d^3x and taking the limit when the volume tends to zero, the continuity equation of equation of mass conservation is obtained:

$$\frac{\partial n}{\partial t} = -\sum \frac{\partial(n\boldsymbol{v_i})}{\partial x_i} \tag{3.12}$$

Written in vector notation and substituting $\boldsymbol{u}$ for $\boldsymbol{v_i}$ as the average velocity, the common expression for the continuity equation for a particle species of the plasma is produced:

$$\frac{\partial n}{\partial t} + \nabla \cdot (n\boldsymbol{u}) = 0 \tag{3.13}$$

This result may also be reached by applying Gauss theorem to the mass exiting or entering the volume.

For this simplified derivation, it is considered that there are no sources or sinks of particles species. This implies that there is no creation of mass in the plasma due to ionization, nor any destruction of mass due to recombination.

Conservation of Momentum

Conservation of momentum requires the differential of momentum with respect to time to be equal to the forces acting on the fluid element. The forces to be considered for a plasma are the electric force field, magnetic force field, pressure forces and the net momentum exchange collisional force, being the gravitational and viscous forces negligible.

To begin with, the momentum of a particle is equal to $m\boldsymbol{u}$, which applied to a volume element is $m\boldsymbol{u}N$, where N is the number of particles contained in the volume, $N = n\Delta V$, being n the particle density. Thus, the left hand side of the momentum conservation equation may be written as:

$$\frac{D}{Dt}(momentum) = \frac{D}{Dt}\left(mn\Delta V\boldsymbol{u}\right) \tag{3.14}$$

This expression is a time material derivative that refers always to the same group of particles, independently of their volume or density change with time.

Eq.3.14 may be re-written by applying the material derivative convention, yielding:

$$\frac{D}{Dt}(momentum) = \Delta V m n \left(\frac{\partial}{\partial t} + \boldsymbol{u}\cdot\nabla\right)\boldsymbol{u} \tag{3.15}$$

To calculate the electric and magnetic field forces the total charge of the infinitesimal volume is required: $Q = qN$, where q is the charge of an individual particle. The electric force is then given by:

$$electric\ field\ force = Q\boldsymbol{E} = \Delta V q n \boldsymbol{E} \tag{3.16}$$

where $\boldsymbol{E}$ is the electric field.

As for the force due to a magentic field, $\boldsymbol{B}$, it is computed as:

$$magnetic\ force\ field = Q\boldsymbol{u}\times\boldsymbol{B} = \Delta V q n \boldsymbol{u}\times\boldsymbol{B} \tag{3.17}$$

The next contribution to the forces acting on the plasma is that of the pressure gradients present in the plasma. To understand the physics of its contribution, it is necessary to observe the individual particles that enter and exit the boundaries of the chosen volume element. The source of pressure gradients is the difference in velocity that exists between particles. Each particle moves at a velocity $\boldsymbol{v} = \boldsymbol{u} + \boldsymbol{w}$, where $\boldsymbol{u}$ is the average velocity and $\boldsymbol{w}$ is the thermal component, which is randomly distributed amongst particles.

To understand the pressure gradient force, it is necessary to observe the flow of thermal momentum crossing the volume's boundaries. Consider a reference frame in which $\boldsymbol{u} = 0$ (Fig. 3.3), any particle just inside the right hand boundary will escape if the x_1 component of the thermal velocity is positive ($w_{x_1} > 0$). This implies a loss of $m\boldsymbol{w}$ momentum for the system. If on the other hand, a particle just outside the volume has a negative thermal momentum ($w_{x_1} < 0$), it shall enter the volume, but also reduce the system's total thermal momentum. A similar process occurs on the left hand side, though in this case, both entering and exiting particles add to the system's momentum. If the increase and decrease of momentum are not of the exact same magnitude, a net variation in momentum will be present in the volume element, which is the source of pressure gradient forces.

To calculate the contribution of these forces, an estimation of the exiting number of particles is necessary. For the right hand boundary, the number of particles leaving will be given by the particle flux times the area:

$$no.\ of\ particles\ leaving = \{[(f_M(\boldsymbol{r},\boldsymbol{w},t)d\boldsymbol{w})(w_x)](\Delta x_2\Delta x_3)\}_{x_1+\Delta x_1/2} \tag{3.18}$$

where $f_M(\boldsymbol{r},\boldsymbol{w},t)$ is the Maxwellian distribution function of the particles.

Once the number of particles exiting the right hand boundary has been estimated, the momentum loss is simply the number of particles exiting times their momentum, that is, (particle flux)(area)($m\boldsymbol{w}$). The equation for loss of momentum can be presented as:

$$loss\ of\ momentum = \left[\Delta x_2\Delta x_3 \int m\boldsymbol{w} w_{x_1} f_M(\boldsymbol{r},\boldsymbol{w},t)d\boldsymbol{w}\right]_{x_1+\Delta x_1/2} \tag{3.19}$$

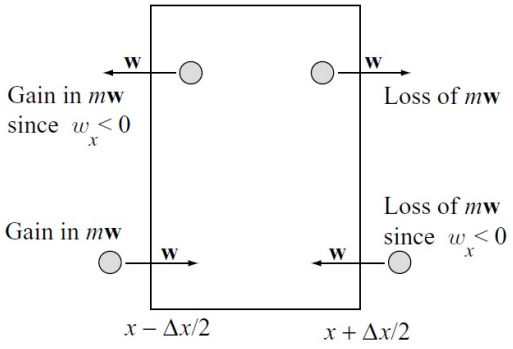

Figure 3.3: Schematic representation of thermal momentum flow in the $\boldsymbol{u} = 0$ reference frame. Source: [6]

considering it once for particles that are exiting the volume and again for particles with negative momentum that are entering. Assuming that the distribution function is, as previously mentioned, Maxwellian, this simplifies the expression and yields the following:

$$\boldsymbol{e_x} \int m w_{x_1}^2 f_M d\boldsymbol{w} = \boldsymbol{e_x} p \tag{3.20}$$

where $p = nT$ is the pressure. If the pressure is multiplied by the area, a force is obtained.

$$total\ loss\ of\ momentum = \boldsymbol{e_x} \Delta x_2 \Delta x_3 p|_{x_1 + \Delta x_1/2} \tag{3.21}$$

$$total\ gain\ of\ momentum = \boldsymbol{e_x} \Delta x_2 \Delta x_3 p|_{x_1 - \Delta x_1/2} \tag{3.22}$$

Finally, the pressure gradient force is the result of calculating the net gain in momentum per unit of time:

$$pressure\ gradient\ forces = \Delta x_2 \Delta x_3 (p|_{x_1 - \Delta x_1/2} - p|_{x_1 + \Delta x_1/2}) \tag{3.23}$$

The same expression expanded to three dimensions is given by:

$$pressure\ gradient\ forces = -\Delta V (\nabla p) \tag{3.24}$$

The final force to be taken into account for the conservation of momentum is the collisional friction force. This force is the result of the friction resultant collisions between two different particle species. The variation of momentum due to this phenomenon is given by:

$$\Delta V m_1 n \frac{d\boldsymbol{u_1}}{dt}|_{collisions} = \Delta V m_1 n \overline{v_{12}} (\boldsymbol{u_1} - \boldsymbol{u_2}) \tag{3.25}$$

with:

$$\overline{v_{12}} = \frac{\sqrt{2}}{12\pi^{3/2}} \frac{e^4 n_i}{\epsilon_0^2 m_e^{1/2} T^{3/2}} \ s^{-1} \tag{3.26}$$

This expression corresponds to the Coulomb collisional frequency, where T is the electron temperature.

Eq.3.25 must be applied to the two populations of the plasma, resulting in forces in opposite directions for ions and electrons.

Now that all forces have been defined, they must be equated to the differential of momentum with respect to time (Eq.3.14) to obtaian the expression of conservation of momentum. As the collisional friction force is different for each species, two different equations shall result, Eq. 3.27 for ions and Eq.3.28 for electrons.

$$m_i n_i \left(\frac{\partial}{\partial t} + \boldsymbol{u_i} \cdot \nabla \right) \boldsymbol{u_i} = q_i n_i (\boldsymbol{E} + \boldsymbol{u_i} \times \boldsymbol{B}) - \nabla p_i - m_e n_e \overline{v_{ei}} (\boldsymbol{u_i} - \boldsymbol{u_e}) \tag{3.27}$$

$$m_e n_e \left(\frac{\partial}{\partial t} + \boldsymbol{u_e} \cdot \nabla \right) \boldsymbol{u_e} = q_e n_e (\boldsymbol{E} + \boldsymbol{u_e} \times \boldsymbol{B}) - \nabla p_e - m_e n_e \overline{v_{ei}} (\boldsymbol{u_e} - \boldsymbol{u_i}) \tag{3.28}$$

Equation of State

In order to close the fluid equations, it is necessary to relate the new unknown, the pressure, with the rest of unknowns through any one of them, for example the density. This can be done by introducing conservtion of the energy or by assuming a simplified polytropic equation of state, which is the approach followed here:

$$p = Cn^\gamma \tag{3.29}$$

where C is a constant value. This expression can be re-written as:

$$pV^\gamma = constant \tag{3.30}$$

In this expression, V is the volume of plasma and γ is a quantity that relates the temperature increase in the plasma with its level of compression as

$$\frac{T}{T_0} = \left(\frac{n}{n_0} \right)^{\gamma - 1} \tag{3.31}$$

The value of γ shall depend on the heat flux assumptions and the energy distribution (isotropic, anisotropic, etc.)

A first case arises when the compression is slow compared to the thermal conduction. This implies that the compression is conducted in an isothermal manner and that $\gamma = 1$. Therefore, any increase in pressure is due solely to an increase in density.

If, on the other hand, compression occurs faster than thermal conduction, it is defined as adiabatic. In this case, $\gamma = (2 + N)/N$, being N the number of degrees of freedom of exchange of collisional energy. Thus, if the compression is adiabatic and $N = 3$, then $\gamma = 5/3$, while for $N = 2$ and $N = 1$, the adiabatic gamma limit assumes the values of 2 and 3 respectively.

Two-fluid Equations

Finally, the set of equations that describe a plasma as two fluids can be obtained from the previous subsections. For each of the species (ions and electrons) the equations are the following:

Conservation of mass

$$\frac{\partial n_j}{\partial t} + \nabla \cdot (n_j \boldsymbol{u_j}) = 0 \tag{3.32}$$

Conservation of momentum

$$m_j n_j \left(\frac{\partial}{\partial t} + \boldsymbol{u_j} \cdot \nabla \right) \boldsymbol{u_j} = q_j n_j (\boldsymbol{E} + \boldsymbol{u_j} \times \boldsymbol{B}) - \nabla p_j - m_j n_j \overline{v_{jk}} (\boldsymbol{u_j} - \boldsymbol{u_k}) \tag{3.33}$$

Equation of state

$$p_j n_j^{-\gamma} = constant \tag{3.34}$$

In this set of equations there are 16 unkowns, corresponding to the densities of each species (n_i and n_e), the average velocity of each species ($\boldsymbol{u_i}$ and $\boldsymbol{u_e}$), the pressure of each population (p_i and p_e) and the electric and magnetic fields ($\boldsymbol{E}$ and $\boldsymbol{B}$). The equations themselves only sum 10 so 6 extra equations must be introduced to have a closed system. Maxwell's equations are introduced for this purpose:

$$\nabla \times \boldsymbol{E} = -\frac{\partial \boldsymbol{B}}{\partial t} \tag{3.35}$$

$$\nabla \times \boldsymbol{B} = \mu_0 \boldsymbol{J} + \frac{1}{c^2} \frac{\partial \boldsymbol{E}}{\partial t} \tag{3.36}$$

$$\nabla \cdot \boldsymbol{E} = \frac{\sigma}{\epsilon_0} \tag{3.37}$$

$$\nabla \cdot \boldsymbol{B} = 0 \tag{3.38}$$

where:

$$\sigma = e(n_i - n_e) \tag{3.39}$$

$$\boldsymbol{J} = e(n_i \boldsymbol{u_i} - n_e \boldsymbol{u_e}) \tag{3.40}$$

Though this may appear to be 8 extra equations, in reality 2 of Maxwell's equations are redundant; the divergence equations may be obtained from Faraday's and Ampere's laws. Therefore, the result is a set of 16 equations for 16 unkowns.

While simpler than kinetic models, the obtained two-fluid model presents a complex coupled and non-linear system that can be further simplified or linearized.

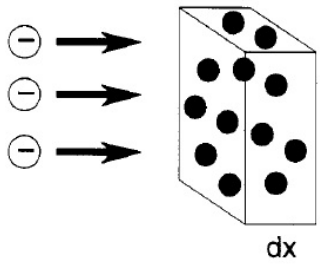

Figure 3.4: Electrons impacting on a slab of thickness dx and density n_a. Source: [5]

3.3 Collision Cross-Sections Basics

Plasma is very much defined by collisions, as a basic source of ionization is collisions between atoms and electrons. However, collisions among charged particles also take place in plasmas, generally dominating when the degree of ionization is high. Thus, it is important to mention some basic parameters that define collisions.

The most important parameter is the collision cross section. Considering a neutral atom colliding with a charged particle, for example an electron, the result can be an elastic or inelastic collision. Independently of the collision effect, the probability that it occurs is defined by an effective cross-sectional area. To further understand the concept, a slab of thickness dx is considered. Inside this slab there is a density n_a of neutral atoms, each of which is assumed a sphere with a cross-sectional area σ. Perpendicular to the slab, electrons are impacting with a flux Γ_0, as shown in Fig.3.4. Knowing this, the fraction of slab area that is occupied by neutral atoms is given by:

$$\frac{n_a A \sigma dx}{A} = n_a \sigma dx \tag{3.41}$$

Therefore, the flux of electrons that passes straight through the slab is:

$$\Gamma_0 + d\Gamma = \Gamma_0(1 - n_a \sigma dx) \tag{3.42}$$

The change of flux along the direction x, throught the slab, is then:

$$\frac{d\Gamma}{dx} = -n_a \sigma \Gamma \tag{3.43}$$

This expression has the following solution:

$$\Gamma = \Gamma_0 \exp(-n_a \sigma x) = \Gamma_0 \exp(-x/\lambda_{mfp}) \tag{3.44}$$

where λ_{mfp} is the mean free path for collision. Mathematically, this describes the distance at which the particle flux is reduced to $1/e$ of its initial value,

which physically corresponds to the distance a particle can travel before it most probably collides with an atom.

$$\lambda_{mfp} = (n_a \sigma)^{-1} \tag{3.45}$$

From the mean free path it is possible to obtain a number of other parameters such as the mean time between collisions or the collision frequency.

The mean time between collisions is the result of dividing the mean free path by the velocity of the charged particle.

$$\tau = \frac{1}{n_a \sigma v} \tag{3.46}$$

The inverse of this quantity results in the collision frequency, which may also be defined in term of the average of all Maxwellian thermal velocities of the charged particles.

$$\nu = \frac{1}{\tau} = n_a \sigma \bar{v} \tag{3.47}$$

These few equation describe a simple case. However, a more complex process, such as a slow moving particle incident on a density of fast moving particles, often results in the cross section, σ, being a function of the relative velocity between the two impacting particles.

3.4 Numerical Techniques Applied to Plasma

Numerical models are applied to many fields of physics as they allow obtaining relatively good results for physical problems that cannot be solved analitically.

In order to simulate the dynamics of a plasma the following items are required:

1. A set of equations that define the plasma evolution (either in terms of fluid variables or single particle motion)
2. A set of equations that define the evolution of the electric and magnetic fields
3. Boundary conditions
4. Initial conditions

Various study approaches can be easily found in literature and are hereafter introduced.

A first approach is to study the plasma with the 2-fluid model. Examples of this are [25] and [30], where the 2-fluid equations are used to compute a plasma plume expansion into vacuum.

In order to investigate aspects of plasmas that cannot be tackled with a fluid approach, kinetic models are generally employed. Such models solve the Boltzmann equations (or a simplified version such as the Maxwell-Vlasov's equation)

numerically to determine how the particle distribution function evolves in time and space. Since the integration has to be performed in both space and velocity coordinates, the numerical effort of directly integrating such equations might be enourmous. For this reason, a simplified kinetic approach, known as "Particle in Cell" method, is generally followed. This approach consists in assuming that the plasma is made up of a large number of computational "super-particles", each representing a large number of ions and electrons. These macro-particles are moved according to Newton's law and determine the electric and magnetic fields through Maxwell's equations, with a dedicated particle weighting algorithm. This method shall be described in detail in the following sections.

Kinetic Vs. Fluid Models

The two-fluid model described in section 3.2 represents a plasma defined by a series of macroscopic variables such as density, fluid velocity, pressure or heat flux. This approach is, as mentioned in section 3.2, more affordable, time and effortwise, than modelling the plasma as a collection of particles. However, fluid models have a series of limitations that render them useless in many frequent situations.

The variables of the fluid model are functions exclusively of $\boldsymbol{x}$ and t, which is a result of assuming that the velocity distribution of each species about the mean velocity is a Maxwellian distribution. This type of distribution is described solely by two parameters, density and temperature. To maintain a Maxwellian distribution, interparticle collisions must be frequent, as occurs for fluids or gases. Nevertheless, the same may not be said of plasmas. Interparticle collision are few in high-temperature plasmas and the plasma found in space is usually considered collisionless. Thus, it is common to have prolonged deviations from local thermodynamic equilibrium which lead to non-Maxwellian velocity distributions.

A strong magnetic field perpendicular to the flow may help maintain the Mawellian distribution in these cases. However, in a low-collisional plasma with an inexistant external magnetic field or with a magnetic field parallel to the flow, the fluid model will diverge from the desired results and correct simulation must be obtained by using a kinetic model.

The kinetic model describes the plasma in terms of a distribution function, that gives the probability of finding each particle at a certain location. The system of Vlasov-Maxwell equations (Eqs.: 3.48, 3.35, 3.36, 3.37, 3.38, 3.39 and 3.40) for the distribution function can be solved to present the motion of the plasma. The Vlasov equation is as follows:

$$\frac{\partial f_j}{\partial t} + \boldsymbol{v} \cdot \frac{\partial f_j}{\partial \boldsymbol{x}} + \frac{q_j}{m}\left(\boldsymbol{E} + \frac{\boldsymbol{v} \times \boldsymbol{B}}{c}\right) \cdot \frac{\partial f_j}{\partial \boldsymbol{v}} = 0 \tag{3.48}$$

where f_j is the distribution function of a species j and $\boldsymbol{x}$ and $\boldsymbol{v}$ are phase space coordinates. This implies that to solve the Vlasov equation, it must be integrated in 6 dimensions. Doing so for the kinetic dynamics of both ions and

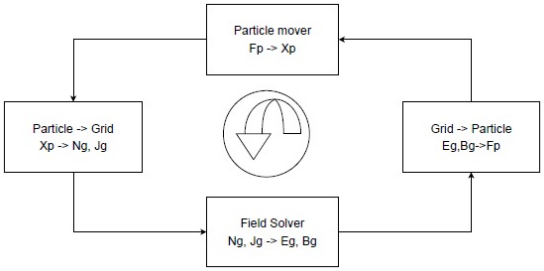

Figure 3.5: Flowchart of the computational cycle of a PIC simulation. Source: [7]

electrons is extremely difficult and time consuming. To overcome this difficulty, a series of solution have been developed, including full PIC simulations and hybrid PIC simulations that are presented below.

Full PIC Simulations

The Particle In Cell (PIC) method simplifies the resolution of the Vlasov equation by considering a finite number of macro-particles that represent the distribution function of the plasma in both velocity and space. In this sense, it represents a statistical approximation to the Boltzmann's equation:

$$f_s(\boldsymbol{r}, \boldsymbol{u}, t) = \sum f_p(\boldsymbol{r}, \boldsymbol{u}, t) \tag{3.49}$$

where f_s is the distribution function of each macroparticle and f_p is the distribution function of each individual particle.

Any PIC simulation consists of four different steps that have been schematized in Fig.3.5, a particle mover, a field solver and two interpolations. The particles move along a continuous domain while their charge and current densities are introduced into a grid by using interpolation methods. The magnetic and electric fields are then obtained by solving Maxwell's equations on the grid points with a standard numerical technique (e.g. finite differences). Interpolating the fields from the grid to the particles' domain produces the forces that move the particles and the process begins again.

The trajectory of a particle is given by the definition of velocity and Newton's second law, where the forces in the case of a charged particle are fruit of the magnetic and electric fields present.

$$\frac{d\boldsymbol{r}(t)}{dt} = \boldsymbol{u}(t) \tag{3.50}$$

$$\frac{d\boldsymbol{u}(t)}{dt} = \frac{q_p}{m_p} \left[\boldsymbol{E}(\boldsymbol{r}, t) + \boldsymbol{u} \times \boldsymbol{B}(\boldsymbol{r}, t)\right] \tag{3.51}$$

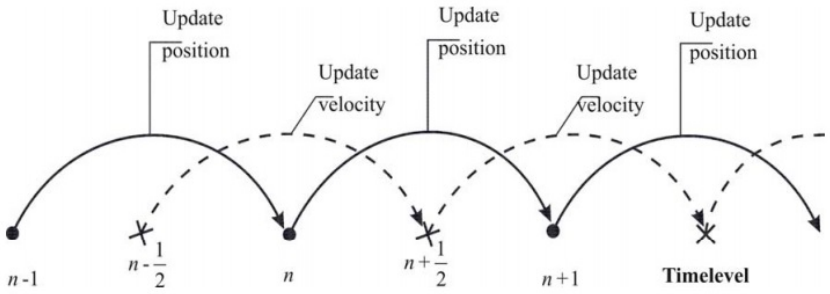

Figure 3.6: Scheme of leapfrog particle position integration. Source: [8]

To move the macroparticles from their position at an initial time step to their position at the next time step two different approaches may be used, an implicit or explicit method. Implicit methods use already updated fields to calculate the position of the particle, while explicit methods make use of the fields obtained in the previous time step, consequently being simpler and faster to compute.

The most commonly used technique, the leap-frog, is an explicit method. It consists in defining position, $\boldsymbol{r}$, and velocity, $\boldsymbol{u}$, with a separation of half an integration time step, as shown in Fig.3.6.

$$\boldsymbol{r}(t+\Delta t) = \boldsymbol{u}(t+\Delta t/2)\Delta t + \boldsymbol{r}(t) \tag{3.52}$$

$$\frac{\boldsymbol{u}(t+\Delta t/2)-\boldsymbol{u}(t-\Delta t/2)}{\Delta t} = \frac{q_p}{m_p}\left[\boldsymbol{E}(\boldsymbol{r},t) + \frac{\boldsymbol{u}(t+\Delta t/2)-\boldsymbol{u}(t-\Delta t/2)}{2} \times \boldsymbol{B}(\boldsymbol{r},t)\right] \tag{3.53}$$

This second expression can be derived to obtain an explicit scheme known as the Boris' CYLRAD algorithm. It is comprised of four expressions which are the following:

$$\boldsymbol{u_1} = \boldsymbol{u}(t-\Delta t/2) + \frac{q_p}{m_p}\boldsymbol{E}\Delta t/2 \tag{3.54}$$

$$\boldsymbol{u_3} = \boldsymbol{u_1} + \boldsymbol{u_1} \times \boldsymbol{\Omega}\Delta t/2 \tag{3.55}$$

$$\boldsymbol{u_2} = \boldsymbol{u_1} + \frac{2\boldsymbol{u_3} \times \boldsymbol{\Omega}}{1+(\boldsymbol{\Omega}\Delta t/2)^2} \tag{3.56}$$

$$\boldsymbol{u}(t+\Delta t/2) = \boldsymbol{u_2} + \frac{q_p}{m_p}\boldsymbol{E}\Delta t/2 \tag{3.57}$$

where $\boldsymbol{\Omega} = \frac{q\boldsymbol{B}}{m}$ is the cyclotron frequency, considered constant for the derivation [35].

Once the position has been obtained, the properties of the particles must be interpolated to the grid or weighted. To do so, the macroparticles are assigned a "shape", which is given by a shape function $S(\boldsymbol{r_p}-\boldsymbol{r})$ where $\boldsymbol{r_p}$ is the position of the particle and $\boldsymbol{r}$ is the observation point or node. With this, it is possible to

obtain the weighting function, W, which determines the fraction of the property value that is assigned to each grid point.

$$W_I(\boldsymbol{r_p}) = \int_{\boldsymbol{r_I - 1/2}}^{\boldsymbol{r_I + 1/2}} S(\boldsymbol{r_p} - \boldsymbol{r}) d\boldsymbol{r} \tag{3.58}$$

where $\boldsymbol{r_I}$ is the grid point of interest.

The weighing function is then used to obtain the number and charge density of a certain species at a determined grid point. There are numerous approaches for this, one of which is the Nearest Grid Point (NGP) method, which consists of assigning the charge of a particle, q_p, to the closest grid point to it. In a 2D Cartesian system, the particle density and charge density at an arbitraty node (x_I, y_J) would be given by the NGP method as:

$$n_{i,j} = \sum_p S(\boldsymbol{r_p} - \boldsymbol{r}) W(\boldsymbol{r_p}) \tag{3.59}$$

$$\rho_{i,j} = \sum_p q_p S(\boldsymbol{r_p} - \boldsymbol{r}) W(\boldsymbol{r_p}) \tag{3.60}$$

This information retrieved at the grid points allows the calculation of the electric and magnetic fields at each grid point. In the case of neglecting the magnetic field, the electrostatic approximation, to solve the electric field only solving Poisson's equation (Eq.3.3) is required. This is done with central differences in a 2D grid such that, for a grid point i, j, the Poisson equation would be expressed as:

$$\frac{\partial^2 \phi}{\partial x^2} + \frac{\partial^2 \phi}{\partial y^2} \simeq \frac{\phi_{i+1,j} - 2\phi_{i,j} + \phi_{i-1,j}}{\Delta x^2} + \frac{\phi_{i,j+1} - 2\phi_{i,j} + \phi_{i,j-1}}{\Delta y^2} = \frac{\rho_{i,j}}{\epsilon_0} \tag{3.61}$$

Expressing the Poisson equation in this manner allows the creation of a matricial problem which is iteratively solved to obtain the potential. From the potential, the electric field is obtained as:

$$\boldsymbol{E} = -\nabla \phi \tag{3.62}$$

Then, the obtained electric field (and if applicable, the magnetic field) must be translated back into the particles' position so as to obtain the forces that produce the movement of the particles.

To do so, the local electric field must be interpolated to the particle location in a manner similar to that used when weighting the particles.

Finally, having obtained the forces acting on the particles, the computational cycle may begin again.

Hybrid PIC Simulations

Hybrid PIC simulations are those in which only one of the two populations of plasma (ions or electrons) is simulated using full PIC simulation, the other is

modelled as a fluid. It is common to find the electrons being simulated as a fluid, as their time and length scales are smaller than those for ions, which is the assumption made in this description of hybrid PIC simulation.

Ions are simulated kinetically using a PIC method. This implies that the ions will be moved according to Eqs.:3.52 and 3.53, providing information of the ion number density and charge density at the grid points that are used to obtain the electric and magnetic field there. They are then interpolated to the particle location to update it.

As for the electrons, they are assumed to be a massless fluid ($m_e = 0$) of constant temperature, governed by the conservation of momentum used for the two-fluid model, Eq.3.28. As was described in section 3.2, the conservation of momentum equation must be accompanied by and equation of state (Eq.3.34) to obtain a relationship between the pressure and temperature.

The assumption of quasi-neutrality in the plasma, that is that the electron and ion charge densities are equal, permits obtaining the density of electrons from the density of ions (valid for singly charged ions):

$$n_e = n_i \tag{3.63}$$

When no magnetic field is present, parting from the momentum conservation equation (Eq.3.64) of the electrons, it is possible to obtain the Boltzmann equation (Eq.3.65) for the density, taking into consideration that the electric potential $\nabla\phi = -\boldsymbol{E}$.

$$m_e \frac{d\boldsymbol{v_e}}{dt} = 0 = qn_e\boldsymbol{E} - k_B T \nabla n \tag{3.64}$$

$$n = n_0 \exp - \left(\frac{\phi - \phi_0}{k_B T}\right) \tag{3.65}$$

This result corresponds to the case in which γ, in the polytropic equation (Eq.3.29), is equal to 1 (isothermal case). However, when γ has a value different to 1, derivation of Eq.3.64 produces:

$$n = n_0 \left(\frac{(\gamma - 1)}{\gamma k_B T}(\phi - \phi_0) + 1\right)^{\frac{1}{\gamma - 1}} \tag{3.66}$$

This is the equation used by SPIS to obtain the potential in the plasma when quasi-neutrality is selected from among the computation options [37].

If, on the other hand, the magnetic field is of relevance in the simulation, a different approach is taken. By solving the momentum conservation equation for the electrons with the assumptions of electrons as a massless fluid and equal density of electrons and ions, a generalized Ohm's law, relating the total electric current with the electric field and the pressure gradient can be obtained.

$$\boldsymbol{E} = \frac{1}{\rho_i}\left[(\boldsymbol{J} - \boldsymbol{J_i}) \times \boldsymbol{B} - \nabla p_e\right] \tag{3.67}$$

This expression may be complemented with Ampere's Law:

$$\nabla \times \boldsymbol{B} = \mu_0 \boldsymbol{J} \tag{3.68}$$

to compute the electric field [38][39]. It is important to keep in mind that $\boldsymbol{J_e} = \boldsymbol{J} - \boldsymbol{J_i}$ and that $\boldsymbol{J_i}$ is obtained through the PIC method applied to the ions.

Finally, in order to advance the value of the magnetic field in time, Faraday's law must be used:

$$\frac{\partial \boldsymbol{B}}{\partial t} = -(\nabla \times \boldsymbol{E}) \tag{3.69}$$

Eq.3.67, 3.68 and 3.69 present the 9 equations required to find the unknowns $\boldsymbol{E}$, $\boldsymbol{B}$ and $\boldsymbol{v_e}$, which relates to the electron current as $\boldsymbol{J_e} = en_e\boldsymbol{v_e}$.

Once the fields have been computed, accelerations can be obtained in order to move the particles.

Monte Carlo Collisions

Monte Carlo methods are applied to a large amount of computations based on random sampling. When referring to plasma, the Monte Carlo method is used to model collisions among particles in the plasma. It is important to simulate interparticle collisions as they are one of the most important effects on the movement of particles. These collisions may be at a long range, described by the Landau-Fokker-Planck equation, or at a short range, described through the Boltzmann equation. The former is the most frequent in plasmas. [40]

Monte Carlo collisions (MCC), one of the simplest methods to model particle collisions, is based on testing every particle to check if a collision occurs, and if so, applying the required action. In general, the procedure determines that a collision will occur if the collision probability of a certain particle is higher than a number obtained randomly. The collision probablity is obtained as:

$$P = 1 - \exp(-\nu\Delta t) = 1 - \exp(-n_n\sigma g\Delta t) \tag{3.70}$$

where n_n is the density of the target gas, σ is the collisional cross-section and g is the relative velocity. Δt is the time step between collision checks, which may be the same as the one used in the PIC method in which the collisions are included, or it may be smaller, to obtain a higher precision [41].

If the test for collision is done between pairs of particles, the method is called Direct Simulation Monte Carlo (DSMC), whereas if the collision occurs between a particle and a target 'cloud', the method is simply called Monte Carlo Collisions. Though the former is more precise and allows for conservation of momentum and energy, its process is slow and cumbersome. Thus, when applicable, MCC is the most effective method.

MCC is generally used in cases in which the density of the target is higher than the density of the source particles, as this results in a low collisional frequency. In other words, MCC is physically applicable when the target is negligibly affected by the collisions occurring, as the method does not conserve

energy. SPIS makes use of MCC to model CEX collisions at the exit of electric thrusters because, as mentioned previously, the density of neutrals in the near region of the plume is higher than that of accelerated ions. In particular the neutral atoms are modeled as a fluid, in which the initial Mach number and the initial mass flow are given as fractions of those of the primary ions. In this context, MCC will define if a collion occurs and the velocity of the collided ion is calculated as:

$$v_{new} = v_{th,n} f_M \tag{3.71}$$

where $v_{th,n}$ is the neutral thermal velocity and f_M is a function that samples the Maxwellian distribution randomly. This process is applied to all source particles including the backflowing ions produced by CEX.

SPIS presents the option of fixing the population of neutrals emitted from the thruster by selecting the temperature of the neutrals and the ratio of neutrals mass flow with respect to ions':

$$\frac{\dot{m_N}}{\dot{m}_i} = \frac{\dot{m_{tot}}}{\dot{m}_i} - \frac{\dot{m}_i}{\dot{m}_i} = \frac{1}{\eta_m} - 1 \tag{3.72}$$

where η_m is the mass utilization efficiency, the ratio ion mass flow with respect to the total mass flow.

Chapter 4

SPIS Tool Description

4.1 General Description of SPIS

The Spacecraft Plasma Interaction Software (SPIS), designed by Onera, Artenum and the University of Paris VII under the contract of ESA, is a software that provides tools which allow modelling and simulating spacecraft-plasma interactions and the charging of spacecraft. It is currently fully functional on Linux, Windows and Mac operating systems.

The SPIS project, initiated in 2002, began with an intention of creating the groundwork for a community based development thereafter, an Open Source software. In this way, the members of the Spacecraft Plasma Interactions Network in Europe (SPINE) have free access to both the software and the source files and may participate with development of plugins and additional features, and with testing.

Structurally, SPIS is divided into two main parts, a numerical integration kernel (NUM) and a graphical user interface (UI). The former is written in Java object-oriented language so as to facilitate modifications and new additions in the simulation process. The latter is required for the user to be able to use the SPIS tool. The UI, which uses Jython, compiles numerous tools for pre-processing, launching the simulation and post-processing of the results, the three main pahses of a SPIS simulation that shall be explained in more detail below.

Pre-processing

The pre-processing phase consists of creating the system to be modelled and thus, is performed prior to any simulation. To do so, the simulation volume must be generated and meshed. On top of this, boundary conditions and simulation properties must be added to provide a complete definition of the system.

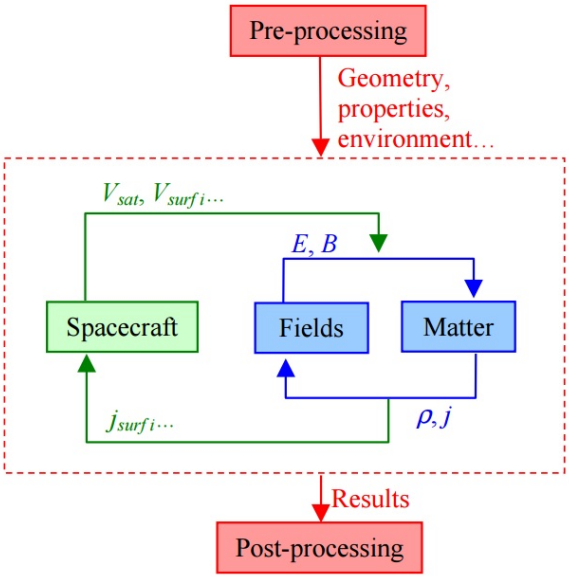

Figure 4.1: Diagram of general simulation process followed in SPIS. Source: [9]

Geometric Modelling and Meshing

For the initial phases of pre-processing, Gmsh, a CAD and meshing tool, is used. It is fundamental for creating an external boundary to the simulation, an internal boundary, which generally corresponds to the spacecraft, and in between the computational volume. This volume is then meshed into unstructured 3D finite elements, whose size will depend on the mesh size chosen when defining each point of the geometry.

Another fundamental aspect of the Gmsh tool is that it permits the creation of Physical Volumes, Surfaces, Lines and Points, which are groups geometrical features that shall later be assigned the same properties.

Local Parameters Definition

Having defined a series of Physicals, the following step is to assign a series of properties to each of these groups. In this way it is possible to define the boundary conditions of the problem and to select characteristics such as materal, electric fields or sources, among others.

Global Parameters Definition

This step consists of selecting the parameters that shall be used in the following step, which is the simulation. The global parameters include values that will

define the space environment, such as plasma properties or the magnetic field, as well as numerical values that will define the simulation, for example the simulation length, time step or solver type.

Once the global parameters are set, the project is converted from the SPIS-UI structure to the SPIS-NUM structure, creating in this way the numerical model for the kernel to simulate.

Simulation

As may be observed in Fig.4.1, the simulation process is divided in two distinct parts, the spacecraft solver (green) and the plasma solver (blue). The spacecraft solver resolves the electric circuit taking into account collected and emitted currents and also the spacecraft's internal electric circuit, that may be defined by the user. This produces values of potentials that are then introduced in the plasma solver as boundary condition values. The plasma solver is subdivided into a field solver and a mattersolver. The field is obtained by applying either a Poisson solver or by assuming quasi-neutrality of the plasma. Using the calculated field, the matter division will create particles and move them throughout the computational volume either applying a PIC method or fluid equations, selected by the user depending on the charging expected. For negative charging, which is present when the spacecraft is in the shade or an ion beam is present (the present case), a hybrid method is generally applied, while for positive charging, which occurs mainly as a consequence of photoemission, a full PIC method is required. The matter division also incorporates MCC to simulate CEX collisions. Then, the plasma solver will provide certain values of density and current [42].

It is important to mention that in the global parameters definition it is possible to define the time step for each population, that is taken into account inside the loops of the simulation process. This is an important optimization technique in cases where the velocities of the various particle types are very different.

Once the simulation is completed, the data generated by SPIS-NUM may be extracted and converted in order to be visualized in the post-processing step.

Post-processing

The various results produced by the simulation include histograms and time series, surface data and volume data. The last two are visualized in 3D using a tool named Cassandra, which is based on the Open Source Visualization Toolkit (VTK). It permits the application of numerous filters, for example Cell Centers that computes an averaged value at the centre of each cell, or the Cutting Plane that displays a planar cut of the computational volume. These filters may be combined to produce very informative graphical outputs.

Finally, SPIS includes an auto-reporting module that generates an Open Office document with all the information regarding the project (input parameters, simulation settings, outputs).

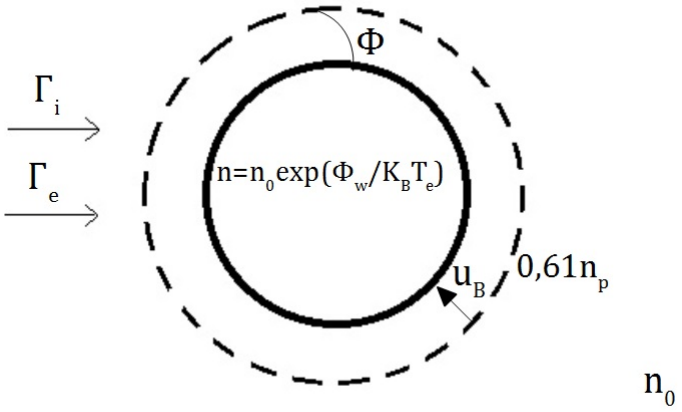

Figure 4.2: Scheme of the validation test.

4.2 Validation Test

With the objective of ensuring the correct functioning of SPIS, a very simple simulation, the charging of a spherical spacecraft with 1 m radius (pictured in Fig.4.2) in a LEO, was carried out with the tool as well as implemented in a Matlab code so as to compare the results.

The Matlab code uses a forward Euler method with a time increment of 10^{-4} s to obtain the spacecraft charge (Eq.4.2) and differential of charge with respect to time (Eq.4.1), which corresponds to the total current. This comprises the ion contribution to the current, which takes into account the Bohm velocity of ions entering the sheath, and the electron contribution, which is calculated with the electrons' thermal velocity.

$$\frac{dQ}{dt}(i+1) = I_i - \frac{eSV_{th_e}}{4} n_0 \exp\left(\frac{Q(i)}{C_{SC}K_BT_e}\right) \tag{4.1}$$

$$Q(i+1) = Q(i) + \frac{dQ}{dt}(i) \cdot dt \tag{4.2}$$

In the above expressions, T_e is the electron temperature equal to 0.1 eV, K_B is Boltzmann's constant, C_{SC} is the capacitance of the spacecraft (assummed to be $1 \cdot 10^{-6}$ F as SPIS provided clearer results setting a value larger than that provided by the formula for the capacitance of a floating sphere), n_0 is the ambient density of plasma equal to 10^{10} m^{-3}, S is the surface of the sphere, e is the charge of an ion and V_{th_e} and I_i are the thermal velocity of electrons and ion current respectively, calculated as:

$$V_{th_e} = \sqrt{\frac{8K_BT_e}{m_e\pi}} \tag{4.3}$$

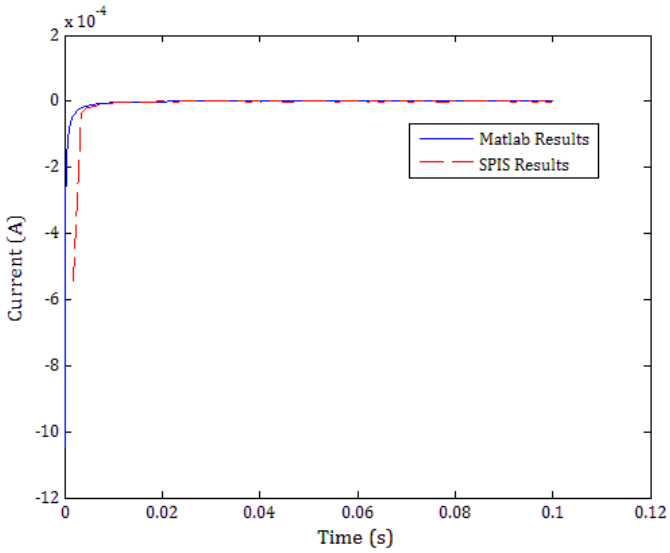

Figure 4.3: Variation of currents in the spacecraft with respect to time.

with m_e equal to the mass of an electron, and

$$I_i = \Gamma_i \cdot S \cdot e \tag{4.4}$$

where Γ_i is the flux of ions on the surface of the spacecraft

$$\Gamma_i = \sqrt{\frac{K_B T_e}{m_i}} \cdot 0.61 \cdot n_0 \tag{4.5}$$

In Eq.4.5, the square root component corresponds to the Bohm velocity, in which m_i is the mass of the ions that are present, oxygen in this case as the spacecraft is in LEO.

The results obtained with this Matlab code are presented alongside those obtained with SPIS in Fig.4.3 and Fig.4.4. For simulating with SPIS, the values used in Matlab were maintained, as was the simulation time. The forward Euler method time step was taken as a maximum value for ion and electron time steps in SPIS. Once again, oxygen ions are considered to be dominant for the modelling.

In Fig.4.3 it is can be seen that the current collected in the spacecraft tends rapidly to zero. When the asymptotic value is reached, it can be assumed that the spacecraft has stabilized at a certain potential value. This value corresponds to the steady-state potential on the wall of a floating spacecraft obtained by substituting the parameters used for the validation test in Eq.3.9. The result, -0.4227 V, is in agreement with the results presented in Fig.4.4.

In both figures it can be appreciated that the difference between computations is neglibly small and, more importantly, that the results obtained are what

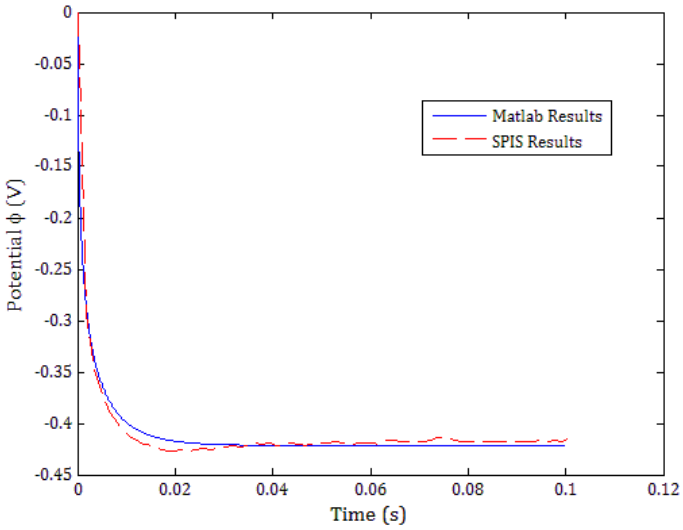

Figure 4.4: Variation of potential in the spacecraft with respect to time.

is expected. Therefore, it is safe to say that the SPIS toolkit is valid for the modelling required in the core of this thesis. The small variations during the transient are due to oscillations in the PIC simulation.

Chapter 5

Definition of the Simulations

5.1 IBS Mission Parameters

The initial step in defining the simulations to be carried out is to fix a series of parameters that are relevant for the IBS and the specific mission that will be modelled. These parameters will be organized in blocks that cover geometry of both the satellite and debris, the mission time, mission-specific data and thruster-related data. The information given will then permit the calculation of other parameters required to define the simulations.

For the sake of clarity, the parameters will be presented again in Table 5.1.

Geometry

Both satellite and target shall be modelled with simple geometries that resemble what will take part in future missions.

The IBS is formed by a cubic central structure with two solar panels, one on each side, as seen in Fig.5.1. The semi-span of the IBS is 5 m long, thus limiting the operational distance to separations > 5 m. Oriented parallel to the solar panels and situated in the centre of one of the cube's faces is the ITT. The thruster has a diameter of 0.1 m and its specific parameters are defined in a following section. The modelling of the ICT is unnecessary as SPIS maintains the distance between satellite and target constant throughout the simulation (e.g. it does not solve the dynamical problem of the IBS-target relative motion).

The debris is modelled as a cylindrical structure, which is similar to many upper stage launchers that are an important source of space junk. The cylinder has a length of 6 m and a diameter of 3 m. It is centered vertically in front of the IBS as seen in Fig.5.1 in order to be as much as possible inside the ion beam.

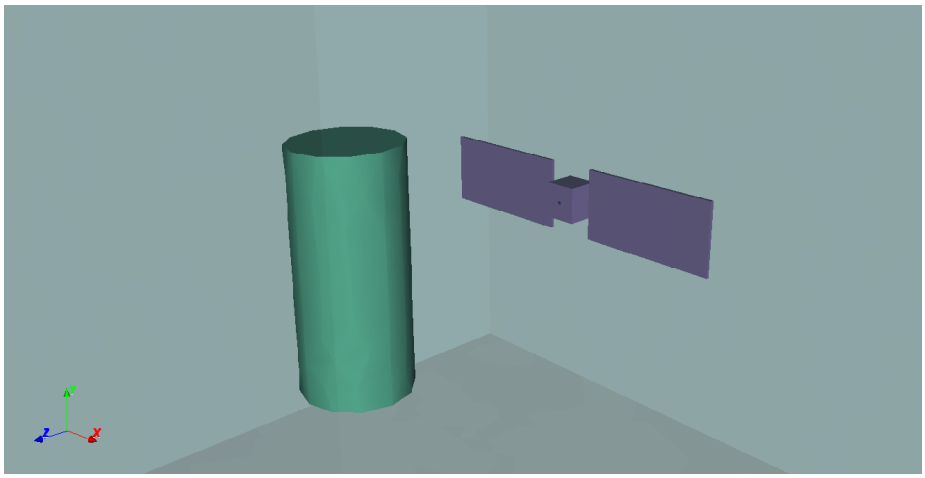

Figure 5.1: Screenshot of the computation geometry taken from SPIS.

Mission Time

To define how long the IBS will be active, it is necessary to select the type of orbit it describes and the duration of the mission.

It is required of the IBS that it deorbit the debris in six months. As a polar orbit has been selected for the satellite, out of the deorbiting time, only a 67% will occur in sunlight. Consequently, as it is powered through its solar panels, during a third of those six months the IBS will be dormant. This leaves a total of 10,419,840 s of active deorbiting.

Mission-specific Data

As well as defining the operation's duration, the operation must be outlined.

The target is considered to be an object with a weight of 1.5 tons. Beginning at an orbital altitude of 800 km, the IBS must push the target to an orbit at which atmospheric drag ensures that the debris' remaining life is of 25 years or less. This corresponds to an altitude of 500 km approximately, which implies a total altitude change of 300 km.

For the sake of simplicity, the initial altitude shall be used in this project to define the orbital velocity, though it is expected to vary in real-life operation. Thus, the constant value of spacecraft (and debris) velocity used is given by the velocity of a circular orbit at an altitude of 800 km:

$$v_c = \sqrt{\frac{\mu}{r}} = 7451.85\ m/s \tag{5.1}$$

where μ is the gravitational constant and r is the radius of the circular orbit. This parameter in SPIS will define the velocity that the IBS and target have with respect to the ambient plasma.

Having taken the velocity corresponding to that of 800 km altitude, the density of the ambient plasma was also taken for that altitude, being a value around 10^{10} particles per m ^{3} [43].

Thruster-related Data

The ITT is an electric ion engine that works with Xenon ions as propellant. A series of parameters related to the engine are defined so as to carry out the simulation.

The specific impulse is a ratio between the thrust of an engine and the rate of propellant it consumes.

$$I_{sp} = \frac{T}{\dot{m} g_0} \tag{5.2}$$

where g_0 is the acceleration of gravity, 9.80665 m/s^2. Typical values of I_{sp} for ion engines lie between 2000 s and 5000 s [44]. An I_{sp} of 4500 s was chosen for this project.

The mass utilization efficiency presents the proportion of the exhaust gas that is ionized.

$$\eta_m = \frac{\dot{m}_i}{\dot{m}} \tag{5.3}$$

A value of 0.9 was selected, meaning that a 10 % of the exhaust flow is composed of neutrals.

The Xenon propellant ions exit the thruster at a certain velocity that is determined with the knowledge of the specific impulse of the engine, I_{sp} and its mass utilization efficiency, η_m. It is also possible to obtain the thruster mass flow rate, the force required on the target and other parameters, which will be computed in the following subsection.

Additional Parameters

With the information provided in the previous subsections it is possible to obtain a series of important parameters, beginning with the force that is required to push the debris to its new orbital altitude.

$$F_t = m_t \cdot \Delta t^{-1} \cdot \Delta v \tag{5.4}$$

where m_t is the mass of the debris, Δt is the time the IBS is active and Δv is the change in velocity experienced from the initial altitude to the final altitude. Considering that the orbits are circular, this is simply the substraction of the two circular orbital velocities, obtained as in Eq.5.1. The resulting force is of $23.167 \cdot 10^{-3}$ N.

Having obtained the thrust required, an approximate calculation of the thruster mass flow using Eq.5.2 yields an exit mass flow of $5.25 \cdot 10^{-7}$ kg/s. It is important to keep in mind that the force acting on the target will only be equal to the force of the thruster if the beam momentum transfer efficiency is equal to one. However, the force acting on the target should provide a close

enough estimate of the mass flow in the case of not knowing the exact value of η_B beforehand.

Direct application of Eq.5.3 with the calculated value of thruster mass flow produces an ion mass flow of $4.72 \cdot 10^{-7}$ kg/s, value which will allow the calculation of the ion beam current as:

$$I_i = \frac{\dot{m}_i \cdot e}{m_i} = 0.347089\ A \tag{5.5}$$

with e being the unit charge and m_i the mass of a Xenon ion. The current flux of the thruster, which is one of the parameters required by SPIS to define the thruster, is obtained simply by dividing the ion beam current by the thruster exit area (a 10 cm diameter is considered) and it is equal to 44.1927 A/m^2.

Finally, the exit velocity of the ions may be computed ignoring the neutrals exiting the thruster, as they are a small portion of the total flow and their velocity compared to the ions' velocity is negligible.

$$v_i = \frac{F_t}{\dot{m}_i} = 49033.2822\ m/s \tag{5.6}$$

Once again, the force used is that applied on the target instead of the force of the thruster itself as the beam momentum transfer efficiency is still unknown.

With the ions' exit velocity, the thruster Mach number, another parameter required by SPIS for the definition of the thruster, is obtained as:

$$M_0 = v_i \cdot \sqrt{\frac{m_i}{T_e \cdot k_B}} = 33.173 \tag{5.7}$$

where k_B is the Boltzmann constant and T_e corresponds to the electron temperature. For the simulation, an electron population with Maxwellian distribution with a temperature of 3 eV is considered.

5.2 Important SPIS Parameters

When defining the simulation in the SPIS user interface, not only the mission parameters were of importance. A series of other parameters, most of which were selected in the 'Global Parameters' section, are fundamental for correct simulation and are described below.

Related to the simulation control, SPIS allows fixing the time step of the simulation, or fixing the maximum permitted time step. In this case, a time step of $1 \cdot 10^{-5}$ s was selected. Also in this section, the duration of the simulation must be introduced, 0.004 s for our simulations.

As for spacecraft parameters, the relative velocity of the spacecraft with respect to the plasma was fixed at the value computed in the previous section, but negative, as the spacecraft is moving in the sense opposite to the positive z axis (this is explained in more detail in section 6.4). SPIS also presents the option to fix a value of the spacecraft capacitance or to compute its exact value

Time variables	Orbit type	Polar
	Shade time (%)	33.00
	Mission duration (months)	6.000
	IBS active time (s)	$1.042 \cdot 10^{7}$
Geometry	IBS half-span (m)	5.000
	Debris length (m)	6.000
	Debris diameter (m)	3.000
Mission parameters	Debris mass (kg)	1500
	Initial altitude (km)	800.0
	Final altitude (km)	300.0
	Orbital velocity (m/s)	7452
	Electron temperature (eV)	3.000
	Plasma density (m^{-3})	10^{10}
Thruster variables	Propellant ions	Xenon
	Specific impulse (s)	4500
	Mass utilization efficiency	0.900
	Exit diameter (m)	0.100
Computed parameters	Force on target (N)	$23.17 \cdot 10^{-3}$
	Thruster mass flow (kg/s)	$5.250 \cdot 10^{-7}$
	Ion mass flow (kg/s)	$4.720 \cdot 10^{-7}$
	Ion beam current (A)	0.3471
	Thruster current flux (A/m^2)	44.20
	Ion exit velocity (m/s)	49030
	Thruster Mach number	33.17

Table 5.1: Parameters required for definition of IBS mission for modelling with SPIS.

at each time step. For this project, a value of capacitance of $1 \cdot 10^{-7}$ F was fixed, as allowing the program to calculate it automatically generated problems in the simulation. Throughout the course of the project, it was also noted that varying the selected value of capacitance affected the time at which the plume reached the debris, that is, it changed the plume propagation speed. A larger value of capacitance increased the plume propagation speed while lower values produced the opposite effect and the selected capacitance resulted in a propagation time similar to that expected taking into consideration the exit velocity of the ions. Nevertheless, such behaviour was completely unexpected and was only found in the simulations in which both the spacecraft and the target debris objects were present. This unphysical behaviour of the simulations was the major cause for abandoning the goal of studying the plasma-bridge interaction.

Surface and volume interactions can be modelled with SPIS if desired. For this project, none of the possible surface interactions (electron secondary emissions, proton secondary emissions, photoemissions and erosion) were activated, as the computational requirements were already high without them. However, volume interactions were necessary, as they define the CEX collisions that will occur in the simulation. The volume interactions section of SPIS' global parameters defines the populations that take part in the CEX collisions and also creates the population of neutrals based on two parameters that define it, the mass flux ratio of neutrals to ions (Eq.3.72) and the temperature at which the neutrals exit the thruster (in eV).

Sources are also managed in the 'Global Parameters' section. It is possible to operate with up to four sources and each source may have up to four subsources. For this project only one source was created and the parameters that defined it (Mach number, current flux and electron temperature) have been developed in the previous section. It is important to note that the type of source must be selected and not all types use the parameters mentioned. However, the chosen source type, MaxwellianThruster, does. It must also be mentioned that a collected current of value equal to the source current flux had to be imposed on the thruster. If this was not done, the spacecraft charged very much and strong potentials developed. This decreased the value of the time step required, to a point where the simulation would no longer run.

Other options SPIS provides include applying a magnetic field to the simulation, using densification factors for populations that have been created automatically and selecting whether a Poisson solver o quasi-neutrality is used to compute the electric field. To model the IBS, the Earth's magnetic field was taken into account, considering it of $4 \cdot 10^{-5}$ T and alligned with the z axis. A densification factor of 100 was used on the population of ions expelled from the source so as to obtain smoother results and the neutrality solver was selected for the electrons.

Once again, for the sake of clarity, these parameters are presented in Table 5.2.

Simulation control	Dt (s)	$1 \cdot 10^{-5}$
	Duration (s)	0.004
Spacecraft	Velocity in z axis (m/s)	-7452
	Capacitance (F)	$1 \cdot 10^{-7}$
Surface interactions	Secondary electron emissions	Off
	Secondary proton emissions	Off
	Photoemissions	Off
	Erosion	Off
Volume interactions	Type of collisions	CEX collisions
	Population 1	Xe+
	Population 2	Xe
	Mass ratio of ions and neutrals	0.111
	Neutrals' temperature (eV)	0.023
Other parameters	Magnetic field in z axis (T)	$4 \cdot 10^{-5}$
	Densification factor of source ions	100.0
	Thruster type	MaxwellianThruster
	Field solver	Quasi-neutrality

Table 5.2: Parameters required for definition of SPIS simulations.

Chapter 6

Results of the Simulations

6.1 Propellant Density

For the simulation to be correct, the first and most important aspect to verify is that the simulated engine presents the expected behaviour, that is, a plume that exits the thruster and advances to reach the target as can be seen in Fig.6.1.

From the instant the plume reaches the target, the debris experiences a sudden increase in its potential and also in the currents it collects (as it begins to receive a current from the propellant ions). For the simulation, though the transitory is of interest, the most important results should be obtained once a steady state condition is achieved. However, some unexpected technical difficulties arised that impeded the SPIS simulation to reach stationary conditions and generate reasonable results. Among these difficulties, the fact that the speed of plume propagation seemed to the depend on the capacitance defined for the full system (IBS plus debris) led to believe that the results obtained for the complete configuration were not reliable and consequently, the results to be extracted were modified in order to obtain information of value.

Swinging the focus of this study to the effect of backflowing ions on the IBS, we then removed the debris from the simulation setup. This action resulted in a simulation in which only the IBS is present and that runs without incidents to stationary conditions. This behavior suggests that SPIS works well only as long as no direct plume impingement with some other solid body of the simulation set takes place.

The plume can be observed in Fig.6.2. As the settings of the engine modelled were the same in each of the simulations, comparison of Fig.6.1 and Fig.6.2 show very similar ion beams, changing exclusively due to the larger simulation time of the latter.

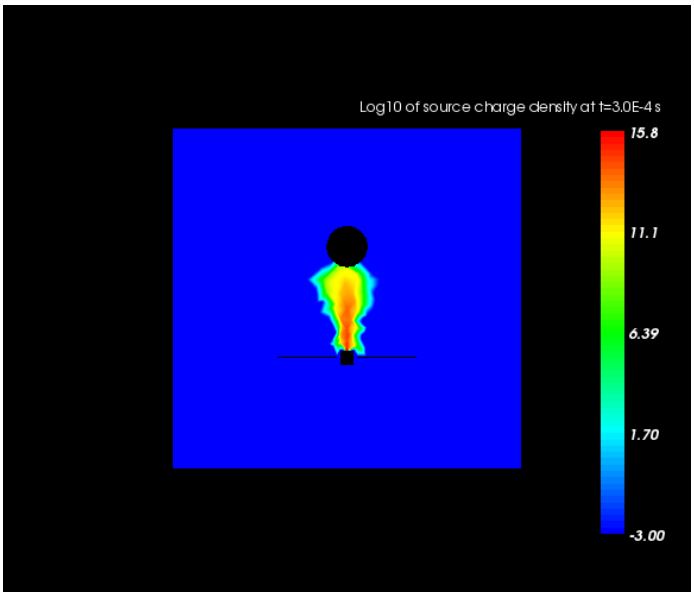

Figure 6.1: 2D view of IBS and debris, showing the $\log_{10}$ of the number density (m^{-3}) of propellant ion particles at $t = 3.0 \cdot 10^{-4}$ s.

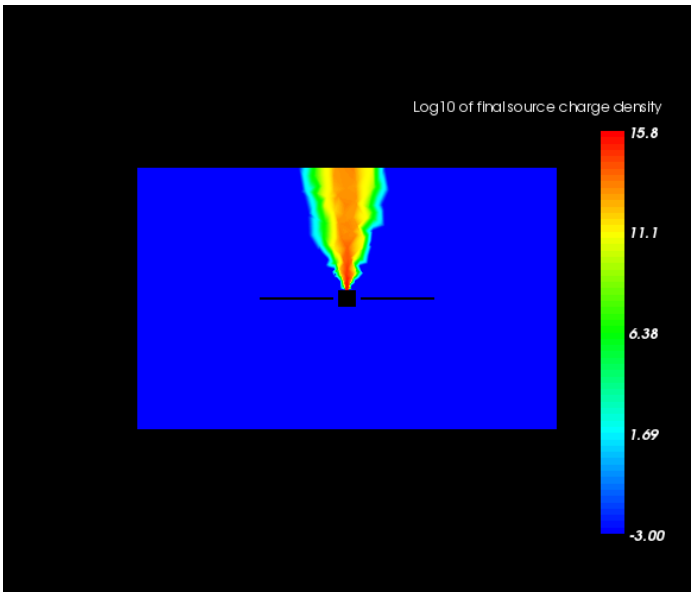

Figure 6.2: 2D view of the $\log_{10}$ of the number density (m^{-3}) of propellant ion particles at stationary conditions ($t = 4.0 \cdot 10^{-3}$ s).

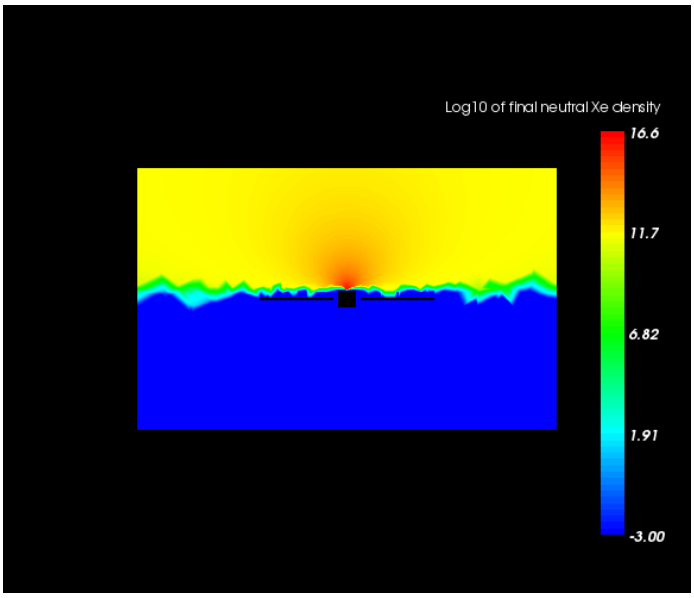

Figure 6.3: 2D view of the $\log_{10}$ of the density of neutral Xenon particles at stationary conditions ($t = 4.0 \cdot 10^{-3}$ s).

6.2 CEX Collisions

Modelling the IBS only and taking into account the ITT is a very simplified simulation, of interest to analyse the appearance of slow ions as a product of CEX collisions and their possible effect on the spacecraft due to backflowing.

The occurence of CEX collisions requires the presence of neutral atoms, in this case, neutral Xe that is not ionized inside the engine. As mentioned previously, the mass utilization efficiency (η_m) is what defines the amount of neutrals that will remain. Having set a value for this parameter (in Chapter 5), the resulting density of neutrals expelled from the ion engine is presented in Fig.6.3. It shows a maximum density of $10^{16.6}$ particles per metre cube next to the engine exit, which decays radially from the thruster outwards.

The wide expansion angle of the particles corresponds to the expansion of neutral particles in vacuum. As the Xe particles are not charged, they exit the thruster at a sonic velocity, much lower than the exit velocity of the propelling ions. This increases their density close to the engine exit in comparison to the charged ions. Thus, this is the zone in which the majority of CEX collisions shall occur.

The amount of slow ions and fast neutrals (though fast neutrals are not simulated in SPIS) that will be created through CEX collisions is defined by:

$$\dot{n}_{CEX} = n_i n_n R \tag{6.1}$$

where n_i is the density of ions, n_n that of the neutrals, and R is the CEX rate.

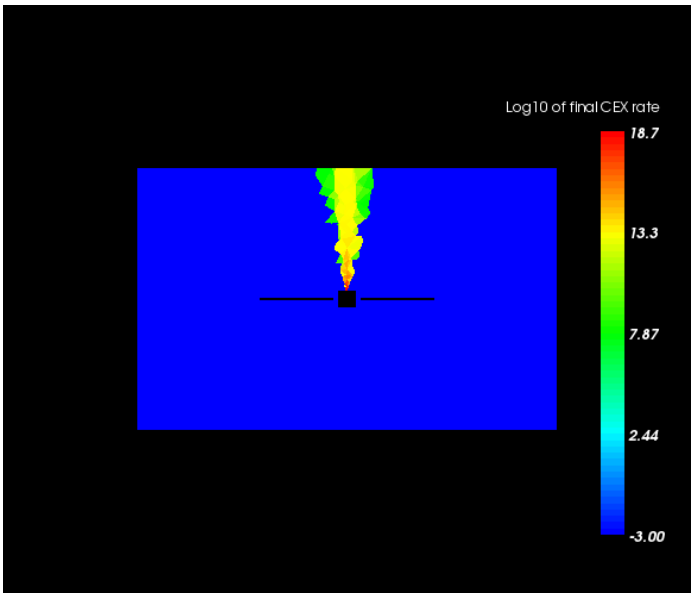

Figure 6.4: 2D view of the $\log_{10}$ of the value of CEX rate ($m^{-3} \cdot s^{-1}$) in stationary conditions ($t = 4.0 \cdot 10^{-3}$ s).

This rate is a function of the CEX cross section, which depends in general on the relative velocity between ions and neutrals (however, as ions are much faster than neutral particles, generally, the velocity of the ions is directly considered). The CEX rate is presented in Fig.6.4, showing, as expected, a high rate close to the engine exit, which rapidly decreases as the density of neutral particles falls.

To complete the evaluation of CEX collisions, the charge density of slow ions generated by SPIS at each collision is presented in Fig.6.5. It is coincident with the results of Fig.6.4, showing that the largest portion of CEX collisions occur close to the thruster. In Fig.6.5, it can be appreciated that the electric fields surrounding the IBS have the sufficient force to veer the slow ions generated in the CEX collisions away from the ion beam and back towards the spacecraft. A stationary condition is reached once the backflowing ions have reached the end of the IBS's solar panels (the IBS is engulfed by slow ions) and from this point onwards, the current flux received by the satelite should become steady, as may be observed in the following section.

6.3 Collected Currents on the Spacecraft

The particles impacting on the surface of the spacecraft may pose a threat to the mission due to contamination mainly. For this reason, the observation of backflowing ions collected on the spacecraft is presented in this section.

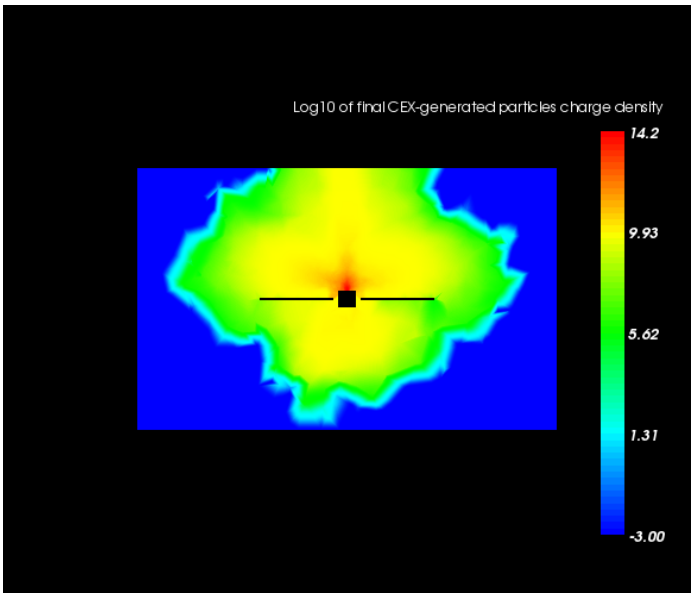

Figure 6.5: 2D view of the $\log_{10}$ of the number density (m^{-3}) of particles that have intervened in a CEX collision at stationary conditions ($t = 4.0 \cdot 10^{-3}$ s).

The manner of observing the amount of backflowing ions that reach the IBS is through the currents that it collects. The simulation was carried out until stationary conditions were reached, evaluated in the current due to backflowing ions collected on the spacecraft surface. Fig.6.6 presents these results with respect to time, showing that a stable value of around $6.4 \cdot 10^{-4}$ A is obtained after 1.5 miliseconds approximately.

At this time, the final distribution of the ions impacting on the spacecraft can be understood from Fig.6.7. The face of the spacecraft body facing the plume is the most affected, while the solar panels present a gradient with more impacts closer to the body, but in general with values between two and five orders of magnitude smaller.

To complement the information obtained from Fig.6.7, four sensors were set up to measure the density of ions reaching them. They were situated on the face of the IBS body in which the engine exits, at the beginning of the solar panel and at the middle section of the solar panel (only on one side as results are symmetrical), as seen in Fig.6.8.

The results, shown in Fig.6.9 confirm those presented in Fig.6.7. Based on these results combined, it would appear that sensors and cameras on the IBS should be placed as far as possible from the ion engine exit to avoid obstruction or degradation due to backflowing ion impacts. However, the amount of backflowing ions along the edge of the spacecraft face is reduced to a third compared to the centre of the face. Thus, if delicate items should be placed on the IBS

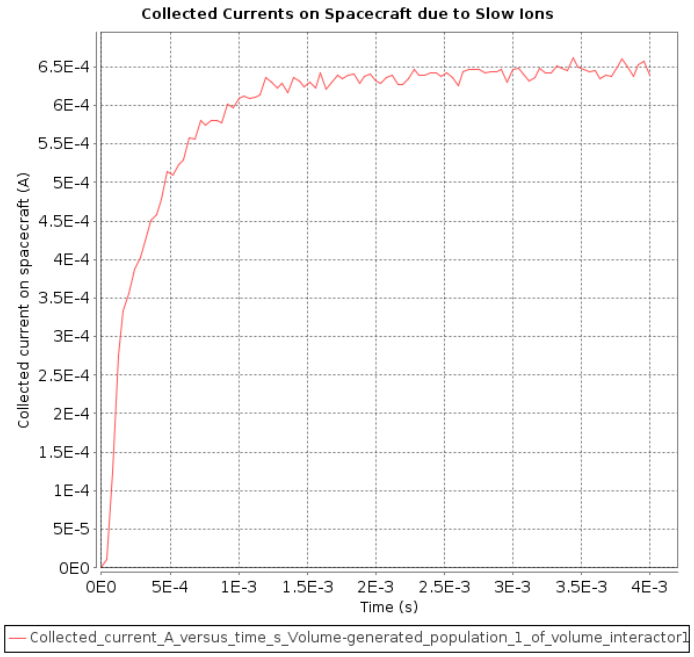

Figure 6.6: Plot of the current of the backflowing ions collected on the spacecraft surface with respect to time.

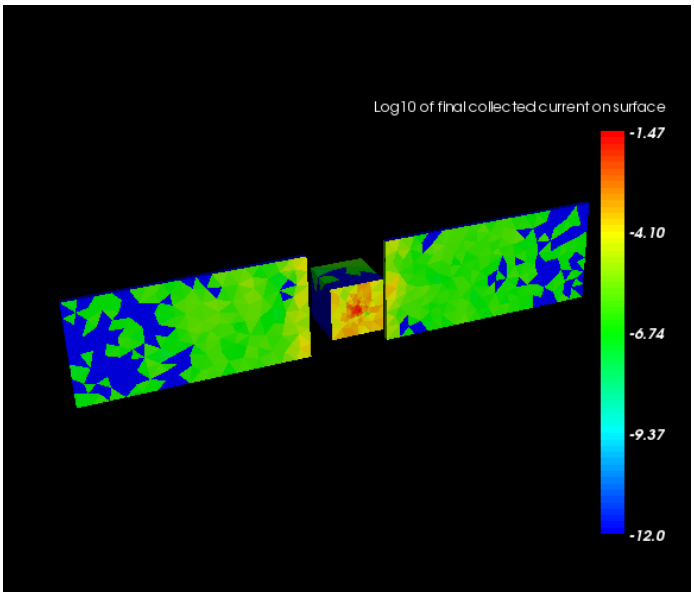

Figure 6.7: 3D view of the $\log_{10}$ of the current ($\mathrm{A/m^2}$) of backtracking ions collected on the spacecraft surface at stationary conditions ($t = 4.0 \cdot 10^{-3}$ s).

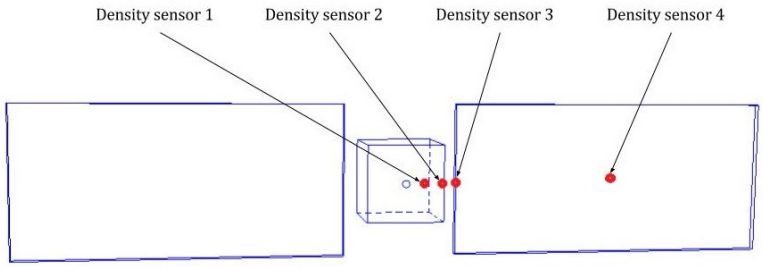

Figure 6.8: Schematic representation of location of density sensors set with SPIS.

facing the plasma plume, the may be fixed as close as possible to the outer edges of the face so as to reduce contamination to a minimum.

It must be noted that Fig.6.9(d) has a different scale along the y-axis compared to the others, as maintaining the scale hindered visualizing the results.

Finally, to calculate the charge that is collected on a hypothetical sensor or camera, a mean kinetic energy sensor was placed at the same spot as the density sensor 2. The readings of this sensor, presented in Fig.6.10, are not constant or smooth. However, the values shown are approximately equal to the potential drop from the centre of the plume to the spacecraft surface, leading to believe that the results are coherent. Taking an approximate mean value of 2.1 eV, it is possible to compute the charge, Q, collected by a sensor of surface S situated at this position as follows:

$$Q = I \cdot t \tag{6.2}$$

$$I = \Gamma_i \cdot S \cdot e \tag{6.3}$$

$$\Gamma_i = v_i \cdot n_i \tag{6.4}$$

where I is the intensity of current, t is the time the sensor is exposed, in this case, the mission duration, Γ_i is the flux of ions, e is the charge of the electron, n_i is the number density of ions and v_i is the velocity of these ions. The density of ions can be taken from Fig.6.9(b) as approximately $8 \cdot 10^{11}$ m^{-3}. The velocity of the ions is extracted from the mean kinetic energy.

$$v_i = \sqrt{\frac{2E_K}{m_i}} \simeq 1750 \ m/s \tag{6.5}$$

This yields a flux of $1.4{\cdot}10^{15} m^{-2} s^{-1}$. Assuming that the hypothetical camera or sensor has a radius of 0.01 m, it will acumulate, throughout one mission of the IBS, 0.7338 C of charge.

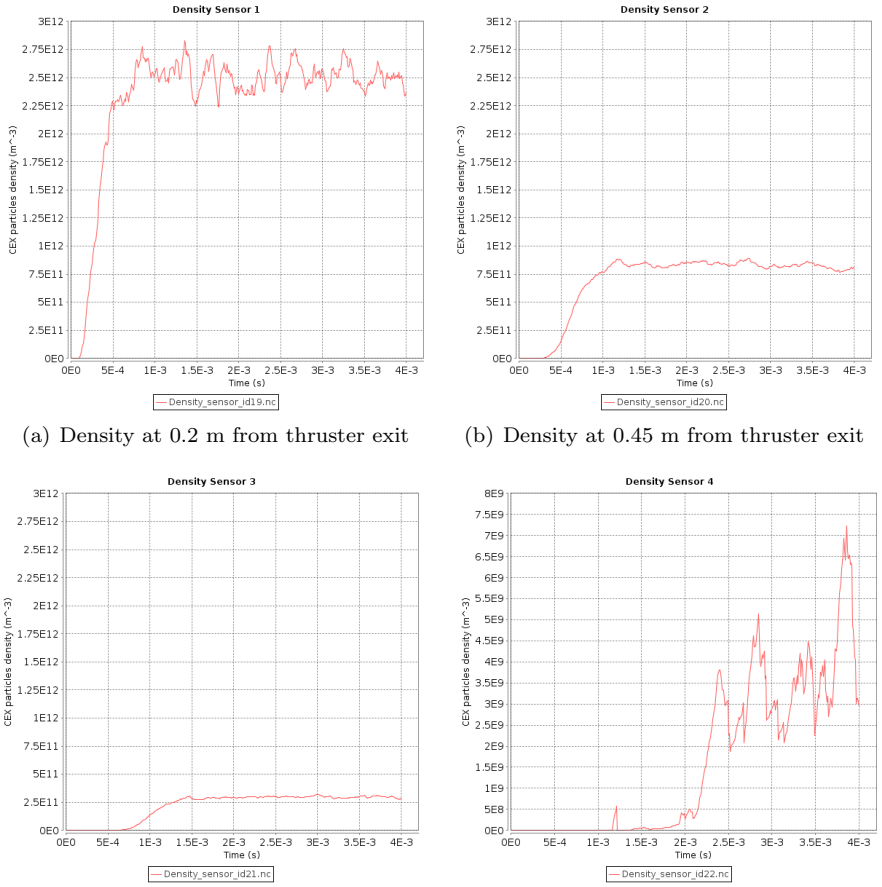

(a) Density at 0.2 m from thruster exit

(b) Density at 0.45 m from thruster exit

(c) Density at 0.7 m from thruster exit

(d) Density at 2.1 m from thruster exit

Figure 6.9: Density of slow ions reaching the spacecraft (m^{-3}).

6.4 Potential of the Plasma

Another aspect of interest in the results obtained is the plasma potential. Fig.6.11 presents the evolution of the plasma potential in time. It can be observed that at the beginning, the velocity of the spacecraft generates a wake in the potential field. The low value of potential behind the solar panels creates intense electric fields that attract the slow ions generated through CEX collisions towards them. This process, in time, varies the potential field such that there is no apparent wake when stationary conditions are reached (Fig.6.12). The potential drop in the plasma plume, both axialy and radially, can be clearly appreciated here.

These results correspond to a de-orbiting task, which is what would be ex-

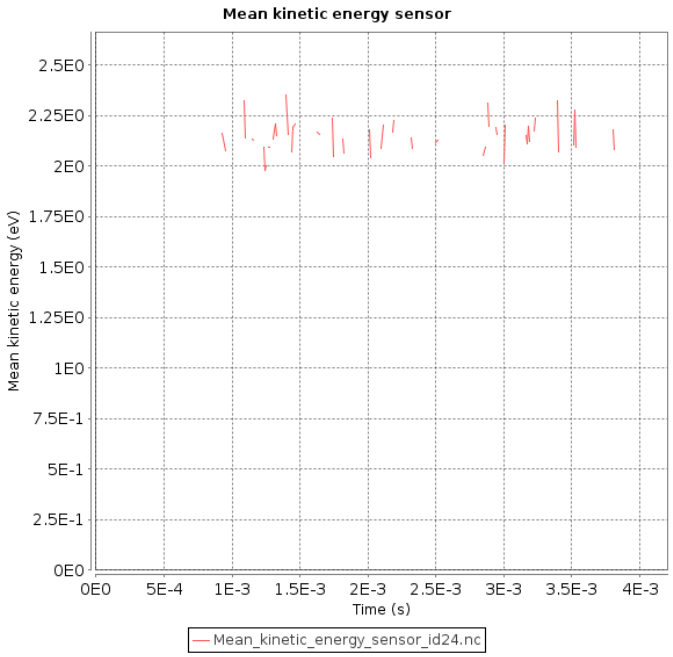

Figure 6.10: Mean kinetic energy (eV) of CEX ions impacting on the edge of the IBS body with respect to time.

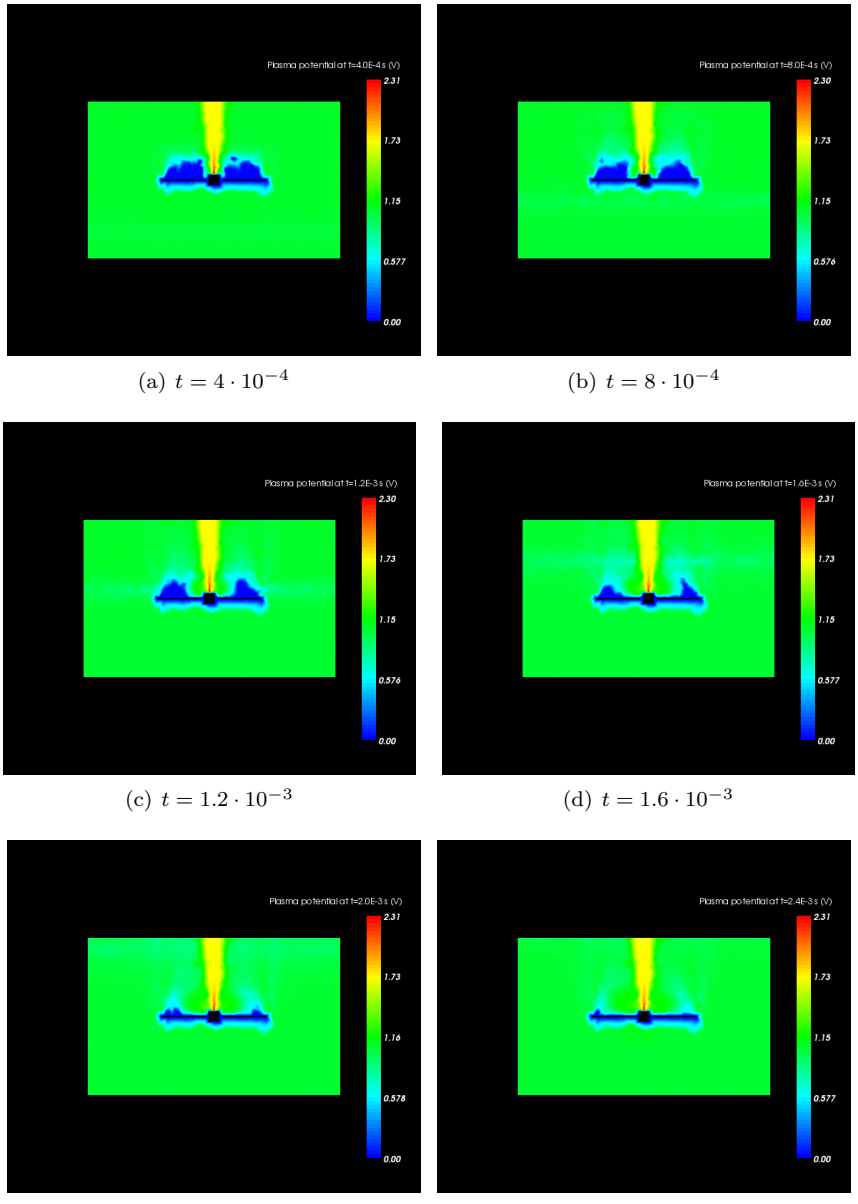

(a) $t = 4 \cdot 10^{-4}$ (b) $t = 8 \cdot 10^{-4}$

(c) $t = 1.2 \cdot 10^{-3}$ (d) $t = 1.6 \cdot 10^{-3}$

(e) $t = 2 \cdot 10^{-3}$ (f) $t = 2.4 \cdot 10^{-3}$

Figure 6.11: 2D view of the temporal evolution of the plasma potential.

pected of the IBS when working in LEO. In the case of re-orbiting of a debris, the results are not the same. In a de-orbiting mission, the IBS must slow down

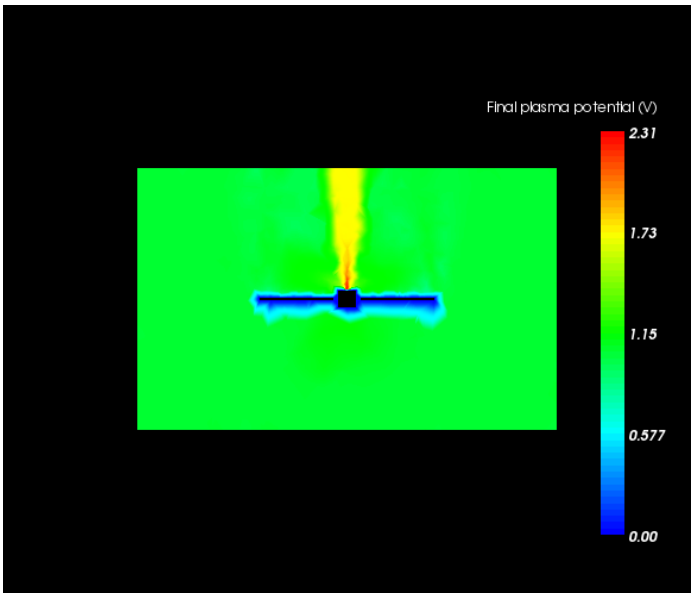

Figure 6.12: 2D view of the potential of the plasma at stationary conditions ($t = 4.0 \cdot 10^{-3}$ s).

the target, thus pointing the beam in a direction opposite to its inertial velocity, whereas for a re-orbiting mission, the opposite configuration applies. This is schematized in Fig.6.13.

The evolution of the plasma potential in the case of a re-orbiting mission is presented in Fig.6.14. It can be seen that the wake of the IBS is now formed on the side of the spacecraft opposite the thruster and it does not recede with time as the density of slow ions generated through CEX is weak in the wake region.

Finally, it is important to note that the wake decreases with altitude and with the plasma density, so that, for a re-orbiting mission at GEO, such considerations would be of little importance.

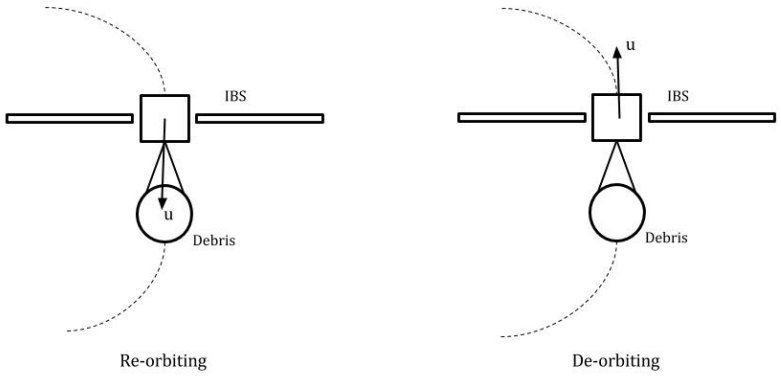

Figure 6.13: Schematic representation of spacecraft velocity in cases of re-orbiting and de-orbiting.

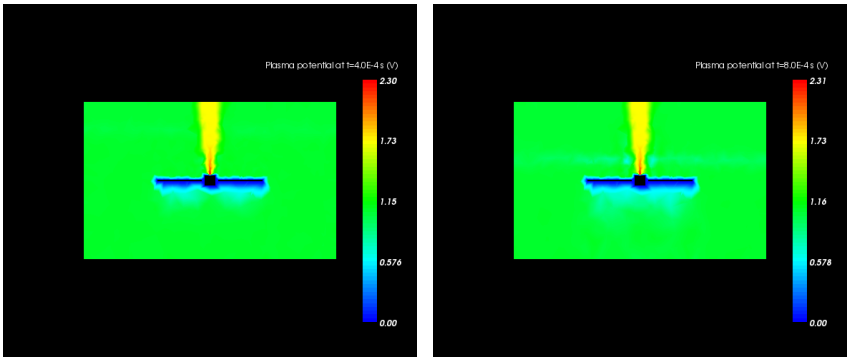

(a) $t = 4 \cdot 10^{-4}$

(b) $t = 8 \cdot 10^{-4}$

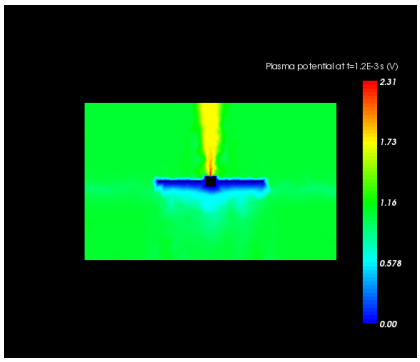

(c) $t = 1.2 \cdot 10^{-3}$

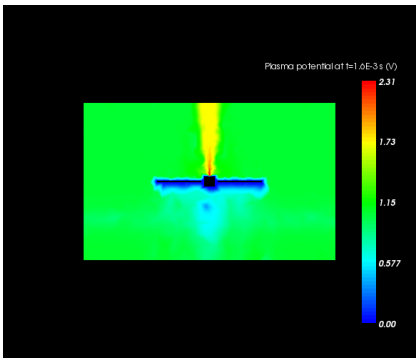

(d) $t = 1.6 \cdot 10^{-3}$

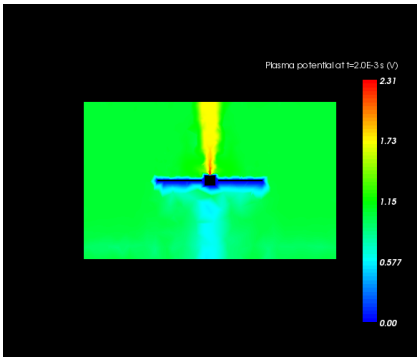

(e) $t = 2 \cdot 10^{-3}$

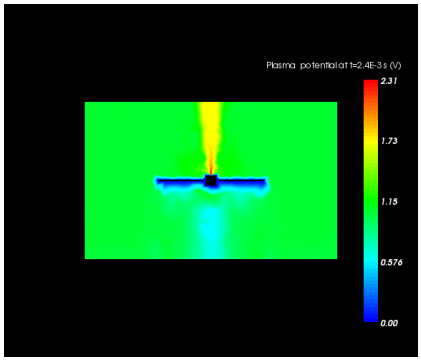

(f) $t = 2.4 \cdot 10^{-3}$

Figure 6.14: 2D view of the temporal evolution of the plasma potential in re-orbiting conditions.

Chapter 7

Conclusions and Future Work

7.1 Conclusions

The work presented in this thesis has been mainly focused on the evaluation of ion backflow towards the IBS. These slow ions are the product of CEX collisions, which generate primarily close to the thruster exit, between propellant ions and propellant gas particles that were not successfully ionized inside the engine.

The IBS was modelled with SPIS and then simulations were launched. The results of these simulations were in agreement with what was expected. It could be observed that the face of the spacecraft body on which the thruster exit is located, is the most affected by back-flow of ion. Receiving a density of up to almost $3 \cdot 10^{12} m^{-3}$, this face presents a poor location to affix sensors or cameras. However, if a location for a delicate piece of engineering must be selected, towards the outer edges of this face, the density of ions is roughly one third of that existing close to the thruster. Along the solar panels, the amount of back-flow decreases gradually outwards, being almost negligible at the solar panel tips.

The CEX ions population has been found to affect sensibly the electric potential distribution around the satellite, making the plasma wake due to the spacecraft orbital motion almost disappear.

Though the initial intention was to calculate, through simulation results, the force that is excerted on the target, the beam momentum transfer efficiency and the differential charging between IBS and debris, several impediments arose that limited the obtainable results. Therefore, these goals are included among the proposals for future work.

Regarding the use of SPIS, it has been found that it is particularly limited when dealing with plumes in general (together with the ion source, an artificial collected ion current had to be added to make the simulation run and avoid the spacecraft to charge electrically) and, more importantly, with direct plume

impingement on a solid body inside the computational domain. The corresponding rapid increase in the potential of such a body made the simulation virtually stop, with no hope of reaching interesting, "stationary" results.

7.2 Future Work

The final results obtained in this bachelor's thesis leave room for a more thorough study of the interaction of the spacecraft with the debris through the ion beam.

Some of the most interesting improvements to this project would be:

1. To include the target debris in the model and to carry out the simulation until stationary conditions are reached. At this point it would be possible to calculate the force acting on the target and from that information, to extract the beam momentum transfer efficiency, η_m. Also, the relative charging between spacecraft and target could be better understood. This task might require some important changes in the SPIS code or the use of techniques that are not described in the public user's manual of the tool.

2. To include the ICT in the model so as to obtain more realistic results of the electric potential surrounding the spacecraft and of the back-flow of ions towards the solar panels and body of the spacecraft.

3. To model the S/C-target system separated by different lengths to study its effect on the beam momentum transfer efficiency.

4. To include photoemissions (electrons generated by the impact of the solar photons with the spacecraft surfaces), as the IBS is only active during the daytime and their presence could significantly alter the results obtained.

5. To simulate erosion in order to observe the effect of the plasma plume on the target debris and any possible back-sputtering towards the IBS.

If these improvements were to be carried out in a hypothetical project, the budget of the project could be defined as follows.

First, a salary must be paid to the engineer working on the project. Prior to the simulations mentioned previously, the employee must become familiar with the software to be used, SPIS. To do so, a course dedicated to studying plume specific issued with SPIS would be of great interest. The cost of such a course could be around €100, but transportation to the site of the course and accommodation and meal costs while there may increase the total cost of taking the course to around €350. Once the engineer feels at ease with SPIS and has validated the tool, which might be after two weeks, the following section of his or her project would be to implement changes in the SPIS code that allow performing the desired simulations. This part of the project would probably be the most time consuming, requiring possibly six weeks. When the SPIS code has been adapted to the project requirements, the goal simulations must be

Basic salary	€7200	Salary of engineer paid €15 per hour for 480 hours of work (including tool validation, modification of SPIS code to fit the project requirements, numerous simulations and processing of results)
SPIS course	€350	Cost of a course on SPIS applied to thruster plumes, displacement of employee, accommodation and meals
Hardware	€800	Desktop computer required for simulations
Software	€500	Supporting software such as an operating system, Office package, etc
Office costs	€2000	Rent, electricity, internet and other costs common to an office environment
Total	€10850	

Table 7.1: Illustrative budget of IBS-target interaction project.

set up and run. An intial estimate of two weeks dedicated to this is plausible. Finally, the obtained results must be understood, processed and presented. For this task, another two weeks may be required. In total, twelve weeks of full time work is intially assigned to this project. Considering a work schedule of eight hours, the employee must be paid for 480 hours of work, at a possible rate of €15 per hour, making a total of €7200.

Secondly, the engineer must work on a computer with a certain software. Supposing that the main software used for this project is SPIS, an expense for this will not be required. However, the computer in use would have an initial cost of €800 and on top of that, basic software required may add another €500 [45].

Finally, the physical space used by the employee must be taken into account. This could vary significantly depending on the status of the worker, but supposing that a shared office is the case, the portion of rent, electricity and other services such as internet or furniture could correspond to around €2000 for the complete duration of the project.

Adding these contributions up, an approximate budget for the project is presented in Table 7.1, resulting in a total of slightly over €10850.

It could also be of interest to recreate experiments in a vacuum chamber to ultimately validate the software in use. However, this could increment the price of the project significantly.

Bibliography

[1] Donald J Kessler, Nicholas L Johnson, JC Liou, and Mark Matney. The kessler syndrome: implications to future space operations. *Advances in the Astronautical Sciences*, 137(8):2010, 2010.

[2] F Cichocki, M Merino, E Ahedo, D Feili, and M Ruiz. Electric propulsion subsystem optimization for" ion beam shepherd" missions. 2015.

[3] J-C Liou. Active debris removal-a grand engineering challenge for the twenty-first century. 2011.

[4] Mercedes Ruiz, E Ahedo, et al. The fp7 leosweep project: Improving low earth orbit security with enhanced electric propulsion. In *Space Propulsion Conference*, 2014.

[5] Robert J Goldston and Paul Harding Rutherford. *Introduction to plasma physics*. CRC Press, 1995.

[6] Jeffrey P Freidberg. *Plasma physics and fusion energy*. Cambridge university press, 2007.

[7] Giovanni Lapenta and Centrum Voor Plasma Astrofysica. Particle in cell methods with application to simulations in space weather. 2013.

[8] Anton M Spirkin. *A three-dimensional particle-in-cell methodology on unstructured Voronoi grids with applications to plasma microdevices*. PhD thesis, Brown University, 2006.

[9] Benoit Thiebault. SPIS home page. `http://dev.spis.org/projects/spine/home/spis`.

[10] LT DeLuca, F Bernelli, F Maggi, P Tadini, C Pardini, L Anselmo, M Grassi, D Pavarin, A Francesconi, F Branz, et al. Active space debris removal by a hybrid propulsion module. *Acta Astronautica*, 91:20–33, 2013.

[11] TS Kelso. Analysis of the 2007 chinese asat test and the impact of its debris on the space environment. In *8th Advanced Maui Optical and Space Surveillance Technologies Conference, Maui, HI*, 2007.

[12] Donald J Kessler and Burton G Cour-Palais. Collision frequency of artificial satellites: The creation of a debris belt. *Journal of Geophysical Research: Space Physics (1978–2012)*, 83(A6):2637–2646, 1978.

[13] NASA. Space debris and human spacecraft. `http://www.nasa.gov/mission_pages/station/news/orbital_debris.html`.

[14] Paula H Krisko. The predicted growth of the low-earth orbit space debris environment—an assessment of future risk for spacecraft. *Proceedings of the Institution of Mechanical Engineers, Part G: Journal of Aerospace Engineering*, 221(6):975–985, 2007.

[15] Luc Moliner. Spot-1 earth observation satellite deorbitation.

[16] Les Johnson, Dean Alhorn, Mark Boudreaux, Joe Casas, Doug Stetson, and Roy Young. Solar and drag sail propulsion: From theory to mission implementation. 2014.

[17] J Peláez, M Sanjurjo, and J Fontdecaba. Satellite deorbiting using a self balanced electrodynamic tether. In *Proceedings of The 55th International Astronautical Congress, Vancouver, Canada,(Paper IAC-04-A. 5.08)*, 2004.

[18] Jeff Foust. Cleaning up space junk. `http://www.thespacereview.com/article/2663/1`.

[19] Kjetil Wormnes, Ronan Le Letty, Leopold Summerer, Rogier Schonenborg, Olivier Dubois-Matra, Eleonora Luraschi, Alexander Cropp, Holger Krag, and Jessica Delaval. Esa technologies for space debris remediation. In *Proceedings of the 6th IAASS Conference: Safety is Not an Option*, pages 3–4, 2013.

[20] M Andrenucci, P Pergola, and A Ruggiero. Active removal of space debris-expanding foam application for active debris removal. 2011.

[21] Christophe Bonnal, Jean-Marc Ruault, and Marie-Christine Desjean. Active debris removal: Recent progress and current trends. *Acta Astronautica*, 85:51–60, 2013.

[22] United Nations Committee on the Peaceful Uses of Outer Space. Space debris mitigation guidelines of the committee on the peaceful uses of outer space. 2010.

[23] Leosweep home page. `https://leosweep.upm.es/en/`.

[24] AG Korsun, EM Tverdokhlebova, and FF Gabdullin. The earth's magnetic field effect upon plasma plume expansion. In *25th Int. El. Prop. Conf*, 1997.

[25] Mario Merino, Filippo Cichocki, Eduardo Ahedo, and Equipo de Propulsión Espacial y Plasmas. Plasma thruster beam expansion and impingement in space debris.

[26] Shoji Kitamura, Yukio Hayakawa, and Satomi Kawamoto. A reorbiter for large geo debris objects using ion beam irradiation. *Acta Astronautica*, 94(2):725–735, 2014.

[27] Samanta Roy and I Robie. Numerical simulation of ion thruster plume backflow for spacecraft contamination assessment. 1995.

[28] C Bramanti, R Walker, O Sutherland, R Boswell, C Charles, P Frigot, M Orlandi, J del Amo, and D Fearn. The innovative dual-stage 4-grid ion thruster concept–theory and first experimental results. In *Fifty-seventh International Astronautical Congress, number IAC-06-C4*, volume 4, 2006.

[29] Juan R Sanmartín et al. Propellantless deorbiting of space debris by bare electrodynamic tethers. 2014.

[30] F Cichocki, M Merino, and E Ahedo. Modeling and simulation of ep plasma plume expansion into vacuum. 2014.

[31] European Space Agency. Spacecraft plasma interaction software (SPIS) introduction. `http://space-env.esa.int/index.php/SPIS.html`.

[32] IH Hutchinson. Introduction to plasma physics. *Lecture Notes, M.I.T.*, 2001.

[33] Dan M Goebel and Ira Katz. *Fundamentals of electric propulsion: ion and Hall thrusters*, volume 1. John Wiley & Sons, 2008.

[34] JD Callen. Fundamentals of plasma physics. *Lecture Notes, University of Wisconsin, Madison*, 2003.

[35] Roger W Hockney and James W Eastwood. *Computer simulation using particles*. CRC Press, 1988.

[36] Trach Minh Tran, Kurt Appert, and Olivier Sauter. A direct poisson solver for particle-in-cell (pic) simulation. Technical report, 1994.

[37] Matthieu Masselin. Development of a hybrid pic code for the simulation of plasma spacecraft interactions, 2012.

[38] Dan Winske, Lin Yin, Nick Omidi, Homa Karimabadi, and Kevin Quest. Hybrid simulation codes: past, present and future—a tutorial. In *Space Plasma Simulation*, pages 136–165. Springer, 2003.

[39] Mats Holmström. Hybrid modeling of plasmas. In *Numerical Mathematics and Advanced Applications 2009*, pages 451–458. Springer, 2010.

[40] Giacomo Dimarco, Russell Caflisch, and Lorenzo Pareschi. Direct simulation monte carlo schemes for coulomb interactions in plasmas. *arXiv preprint arXiv:1010.0108*, 2010.

[41] Charles K Birdsall. Particle-in-cell charged-particle simulations, plus monte carlo collisions with neutral atoms, pic-mcc. *Plasma Science, IEEE Transactions on*, 19(2):65–85, 1991.

[42] Nuno Loureiro. Modelling of plasma thruster plumes for spacecraft plume impingement analysis, 2010.

[43] Michael C Kelley. *The Earth's Ionosphere: Plasma Physics & Electrodynamics*, volume 96. Academic press, 2009.

[44] George P Sutton and Oscar Biblarz. *Rocket propulsion elements*. John Wiley & Sons, 2010.

[45] Joe Hadzima. " how much does an employee cost? *Boston Business Journal*, 2011.